Journal of Medicinal Chemistry

pubs.acs.org/jmc Article

Photoswitchable Antagonists for a Precise Spatiotemporal Control of β_2-Adrenoceptors

Anna Duran-Corbera, Juanlo Catena, Marta Otero-Viñas, Amadeu Llebaria,* and Xavier Rovira*

Cite This: J. Med. Chem. 2020, 63, 8458−8470 Read Online

ACCESS | Metrics & More | Article Recommendations | Supporting Information

ABSTRACT: β_2-Adrenoceptors (β_2-AR) are prototypical G-protein-coupled receptors and important pharmacological targets with relevant roles in physiological processes and diseases. Herein, we introduce **Photoazolol-1−3**, a series of photoswitchable azobenzene β_2-AR antagonists that can be reversibly controlled with light. These new photochromic ligands are designed following the azologization strategy, with a *p*-acetamido azobenzene substituting the hydrophobic moiety present in many β_2-AR antagonists. Using a fluorescence resonance energy transfer (FRET) biosensor-based assay, a variety of photopharmacological properties are identified. Two of the light-regulated molecules show potent β_2-AR antagonism and enable a reversible and dynamic control of cellular receptor activity with light. Their photopharmacological properties are opposite, with **Photoazolol-1** being more active in the dark and **Photoazolol-2** demonstrating higher antagonism upon illumination. In addition, we provide a molecular rationale for the interaction of the different photoisomers with the receptor. Overall, we present innovative tools and a proof of concept for the precise control of β_2-AR by means of light.

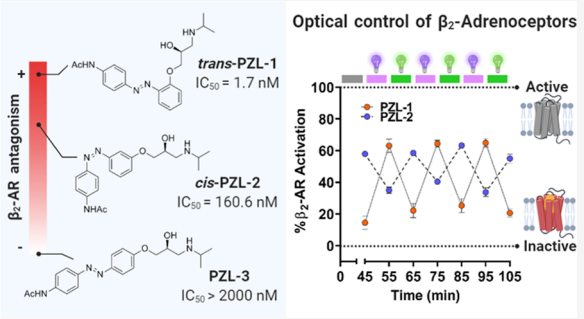

INTRODUCTION

Photopharmacology is an emerging field of research based on the use of light-regulated drugs.[1] In the past years, a number of photocontrollable molecules have been reported, showing their ability to modulate the activation state of several G-protein-coupled receptors (GPCRs).[2] Interestingly, unprecedented research involving GPCR photopharmacology with diffusible drugs has demonstrated the performance of this chemical approach to dynamically manage physiological conditions in rodents, including the abolition of the physical and emotional symptoms of persistent pain.[3,4] These and other recent studies highlight the enormous potential of photopharmacology for the study of GPCR roles in physiological processes and the development of future precise drugs.[5]

Mainly, two different chemical strategies have been used in photopharmacology to design diffusible molecules that allow a spatiotemporal localization of the drug action. The first, named compound caging, is based on the transformation of biologically active molecules into inactive compounds through the attachment of a photolabile protecting group to their chemical structure, which abolishes their binding within the receptors. The protecting groups are irreversibly cleaved upon illumination, thus causing a local release of the drug that subsequently acts following conventional pharmacology patterns.[6] Therefore, the activity of caged compounds is not reversible, which limits the temporal regulation of the bioactive molecule once released and may cause possible side effects in adjacent tissues. The second approach is based on the introduction of a photochromic moiety within a drug structure to reversibly adjust its activity with light.[7,8] From the four most typical classes of photochromic moieties (azobenzenes, dihydropyrans, diarylethenes, and fulgides), azo-based compounds have been widely applied in the context of GPCR photopharmacology to date.[2] The reversible conversion of the compound between two states by light illumination produces changes in the polarity, geometry, and end-to-end distance. These light-regulated changes in the molecule can be designed to alter its functional properties as a ligand (e.g., agonist/antagonist character) or the accessibility to its binding site within the receptor (affinity).[9] In principle, with photoisomerizable molecules, the selectivity of the drug action can be finely tuned by a rapid thermal relaxation to the most stable state or using a different light wavelength to switch on and off its activity. In addition, the concentration of the active isomer can be adjusted by modulating the light power or the wavelength used.[7,10] Today, the GPCR photopharmacological toolbox includes a variety of pharmacological and chemical strategies, including photoswitchable tethered ligands,[11] ligands acting as agonists or antagonists depending on the applied light,[9,12] photoswitchable dualsteric ligands,[13] light-

Received: May 15, 2020
Published: July 20, 2020

https://dx.doi.org/10.1021/acs.jmedchem.0c00831
J. Med. Chem. 2020, 63, 8458−8470

regulated ligands based on dithienylethenes and fulgides,[14] ligands that can be activated using two-photon excitation with near-infrared light,[15] ligands more active in the dark[16,17] and others in the less stable photoisomeric state upon illumination,[18] among others. Overall, the development of photoswitches to regulate GPCRs with light is an emerging field and may open new avenues for the treatment of many diseases with unmet needs in innovative ways that are not possible with classical pharmacology.[1,5]

GPCRs are major pharmacological targets accounting for around one-third of the marketed drugs.[19] Among this family, β-adrenoceptors are prototypical GPCRs and molecules directed toward these receptors, either agonists or antagonists, are first-line treatments for important diseases, such as several heart dysfunctions, asthma, anxiety, urinary incontinence, migraine, glaucoma, among others.[20,21] Therefore, developing light-regulated strategies to activate or inactivate β-adrenoceptors in a controlled manner can be of great research and therapeutic interest. To date, several studies have been directed to control the activity of β_2-adrenoceptors (β_2-AR) with light. Indeed, caged derivatives based on adrenergic receptor agonists were developed.[22] Also, a caged version of the antagonist Timolol has been recently synthesized cross-linked on a polymer surface to build contact lenses, which may have applications for the treatment of intraocular pressure in patients with glaucoma.[23] Using a very different approach, a research study presented a chimeric β_2-AR construct that could be controlled by light (opto-β_2AR). This construct was composed of the light-sensitive region of rhodopsin and the G_s-coupling region of β_2-AR.[24] The authors demonstrated that this biotechnological tool could be applicable for the light control of cyclic adenosine monophosphate (cAMP) levels in cell cultures, native tissues and could even modulate behavior in freely moving mice.

Despite the interesting prospects of caged compounds and light-regulated chimeric constructs, major drawbacks, such as the irreversible nature of caged compounds or the need to genetically modify the organism, hamper their precise use in physiological environments. In this context, using a new approach based on photoisomerizable molecules targeting β_2-AR could provide a valid alternative with therapeutic and research potential. The present work provides the first proof of concept for reversible β_2-AR photopharmacology. We present two photoswitchable compounds that antagonize β_2-AR agonist activity in a light-dependent manner. Biological *in vitro* testing highlights the successful development of two compounds with promising pharmacological properties that can be reversibly controlled in opposite ways, either increasing or reducing their β_2-AR activity upon illumination.

RESULTS AND DISCUSSION

Design, Synthesis, and Photochemical Characterization of Photoswitchable β_2-Adrenoceptor antagonists. The chemical design of photoswitchable compounds targeting β_2-AR was based on the 3-aryloxypropan-2-olamine molecular scaffold commonly found in β-adrenoceptor antagonists (Figure 1). Noticeably, these molecules are constituted by an aromatic ring connected to an ethanolamine backbone through an oxymethylene bridge. It is well described that the ethanolamine moiety plays an essential role in the ligand−protein interaction, considering that it forms H-bond interactions with key residues on the binding pocket.[25] Additionally, compounds incorporating the oxymethylene

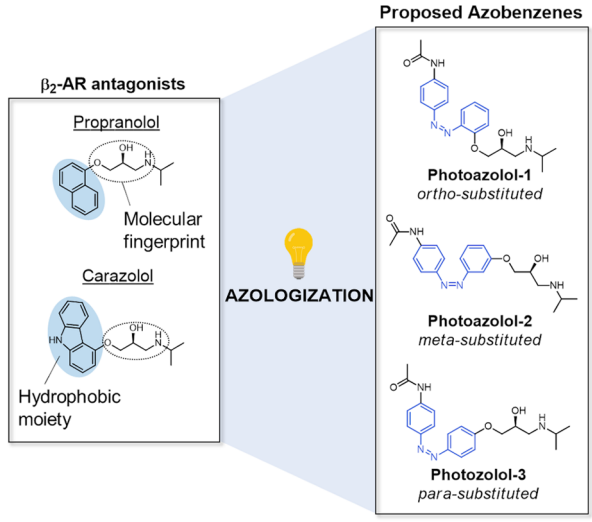

Figure 1. Design of photoswitchable azobenzene β_2-AR antagonists photoazolols (PZLs). Left panel, prototypical β-adrenoceptor antagonists. Right panel, designed photoisomerizable molecules following the azologization strategy.

bridge on their structure have been signaled as β-adrenoceptor antagonists. Therefore, the relevance of the oxyaminoalcohol substructure in ligand function highlights it as the so-called molecular fingerprint of β-adrenoceptor antagonists.[25] On the other hand, the hydrophobic moiety admits certain variations as it can integrate multiple aromatic fused rings or heteroaromatic substructures (e.g., carbazole and indole). Consequently, we identified the hydrophobic core as suitable for the azologization strategy.[26] We proposed three different molecules, where the naphthalene of propranolol and the tricyclic carbazole moiety of carazolol are substituted for an azobenzene moiety. The designed azobenzenes are structural isomers, where the only difference relies on the aromatic substitution pattern of the oxyaminoalcohol with respect to the N═N bond (Figure 1).

Importantly, the vast majority of ligands targeting β_2-AR are chiral. In fact, different pharmacological behaviors have been distinguished for the enantiomers, with better β_2-AR pharmacological properties always observed for the (*S*)-eutomers.[27] Therefore, and according to the structure of potent ligands, we aimed to synthesize the (*S*)-enantiomers of the designed azobenzenes. Finally, all azobenzene compounds were designed with a *p*-acetamido substituent, which was introduced with the objective to obtain photochromic ligands with appropriate photochemical properties.[28]

The synthetic routes developed to produce photocontrolled β_2-AR antagonists are depicted in Scheme 1. All three routes share an analogous intermediate, which is the phenolic azobenzene (**5**, **6**, and **10**). Direct diazotization of the *p*-acetamidoaniline (**4**) followed by a reaction with phenol yielded phenylazophenolic intermediate **6**. Nevertheless, synthesis of the *meta*- and *ortho*-acetamido intermediates **5** and **10** was conducted via the typical Mills reaction involving condensation of appropriate anilines and aromatic nitroso compounds. This alternative procedure was explored after the attempted diazotization of the respective aminophenols proved unsuccessful. Thus, *ortho*-phenolic azobenzene **10** was obtained by oxidation of the *p*-acetamidoaniline (**4**) to the corresponding nitroso compound (**9**), followed by Mills condensation with 2-aminophenol. On the other hand, it is

https://dx.doi.org/10.1021/acs.jmedchem.0c00831
J. Med. Chem. 2020, 63, 8458−8470

Scheme 1. Synthesis of Photoazolol-1−3[a]

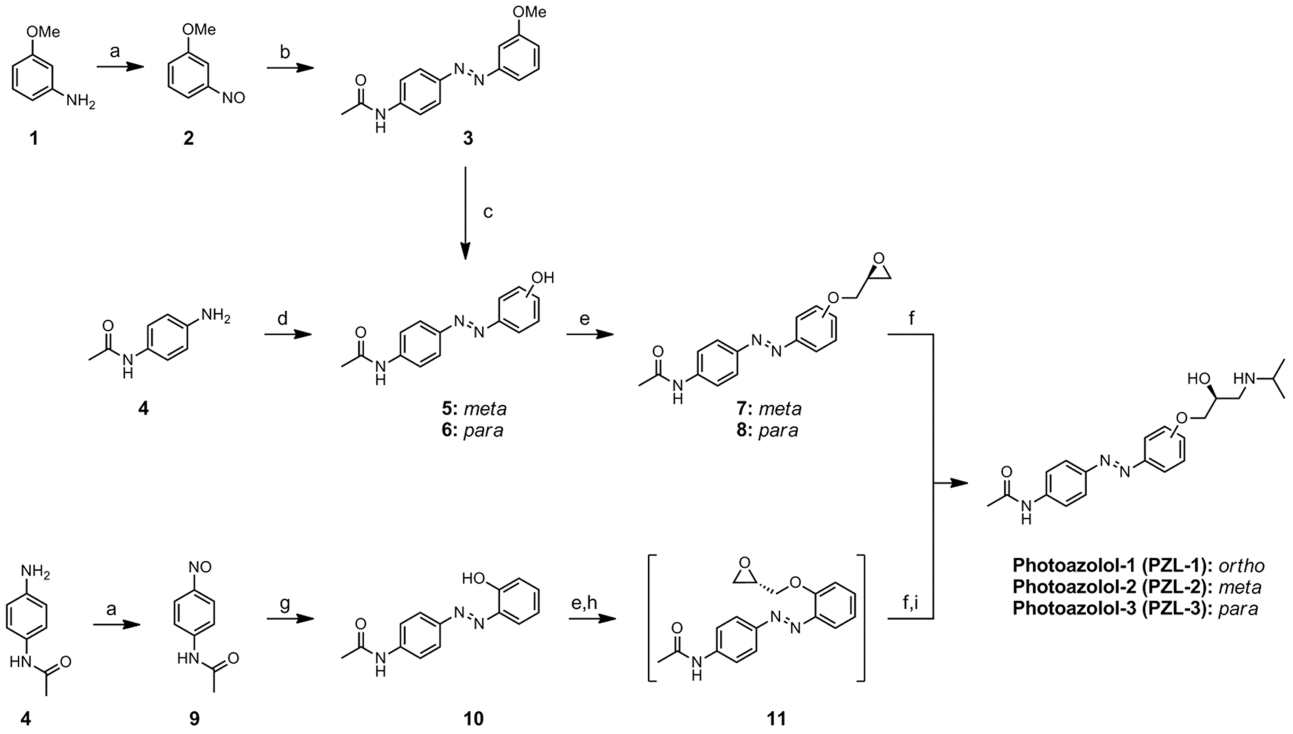

[a]Reagents and conditions: (a) oxone, H_2O/DCM 1:1, rt, 2 h; (b) *p*-acetamidoaniline, AcOH, rt, 48 h, 25−41%; (c) BBr_3, dichloromethane (DCM), 0 °C to rt, 24 h, 95%; (d) (I) $NaNO_2$, aq HCl, 0 °C, 5 min; (II) phenol, aq NaOH, 0 °C, 30 min 63%; (e) (*R*)-epichlorohydrin, K_2CO_3, butanone, reflux, 48 h, 59%-quantitative; (f) *i*-$PrNH_2$, 12 h, rt, 29−56%; (g) 2-aminophenol, AcOH, rt, 48 h, 16−21%; (h) (2*S*)-glycidyl tosylate, K_2CO_3, dimethylformamide (DMF), rt, 12 h; and (i) *i*-$PrNH_2$, 90 °C, 48 h, 33%.

worth noting that to produce *m*-phenolic azobenzene **5** a methoxy protected intermediate **3** had to be synthesized. The condensation of the nitrosoacetamide with 3-aminophenol proceeded with very low yields. In consequence, 3-methoxyaniline (**1**) was oxidized to the nitroso derivative (**2**) and reacted with the *p*-acetamidoaniline (**4**) to yield azobenzene **3**. Subsequent *O*-demethylation in **3** using BBr_3 led to the desired azobenzene intermediate **5** in good yield.

Once the key intermediates were synthesized, the following steps required the use of enantioselective reactions to afford the (*S*)-enantiomers of **PZL-1−3**. To obtain the proposed light-regulated β_2-AR antagonists, we initially followed a commonly reported route for the synthesis of β_2-AR antagonists.[29] The phenolic azobenzenes were alkylated by direct reaction with (*R*)-epichlorohydrin. This reaction, using either acetone or butanone as a solvent, proceeds with the inversion of configuration to yield (*S*)-oxiranes.[29] The epoxides were finally opened by nucleophilic attack of isopropylamine. This route provided azobenzenes **PZL-2** and **-3** with good enantiomeric purity. In contrast, the *ortho*-substituted product was found to be partially racemized. The exact reasons for this behavior in the *O*-diazenylphenol **10** remain unknown. To overcome this difficulty, a different enantioselective route reported for the production of (2*S*)-propranolol was explored.[30] This new approach consists of a one-pot reaction of phenol **10** using (2*S*)-glycidyl tosylate and isopropylamine as main reagents. Regioselective displacement of the tosylate moiety by phenol under mild basic conditions afforded the epoxyether intermediate (**11**) that was not isolated. Epoxide opening was thereafter effected by refluxing the reaction mixture with isopropylamine to give **PZL-1** with good enantiomeric purity.

Following the synthesis of the desired compounds, the photochemical properties of **PZL-1−3** were evaluated. To be able to effectively control β_2-AR with light, it is an essential requisite to find specific light parameters to interconvert *trans* and *cis* azobenzenes in both directions with high isomeric conversion ratios and in a relatively fast manner with respect to the receptor activation kinetics. Results from the photochemical characterization of the obtained azobenzenes are summarized in Table 1. General tendencies can be observed for the three azobenzenes. Suitable isomerization from the thermostable *trans* to the *cis* configuration occurs when applying near-ultraviolet light (365/380 nm). Compounds can also be back-isomerized to their thermally stable isomer using green-yellow light (525/550 nm) (Figures 2 and S1−S5).

Table 1. Photochemical properties of Photoazolols-1−3[a]

compound	λ_{trans}[a] (nm)	λ_{cis}[a] (nm)	$t_{1/2}$[a] (min)	PSS_{380}[b] (% *cis*)	PSS_{550}[b] (% *trans*)
PZL-1	356	428	72.6	86.2	71.4
PZL-2	350	430	152.1	87.7	77.5
PZL-3	360	440	169.4	94.3	86.2

[a]Determined at 50 μM in aqueous buffer + 0.5% dimethyl sulfoxide (DMSO), 25 °C. [b]Photostationary state (PSS) ratios were determined at 12 °C by ^{1}H NMR after illumination (380/550 nm) of a 100 μM sample in D_2O.

Importantly, conversion ratios from *trans* to *cis* isomers are higher than 86%. Nevertheless, back-isomerization occurs with

https://dx.doi.org/10.1021/acs.jmedchem.0c00831
J. Med. Chem. 2020, 63, 8458−8470

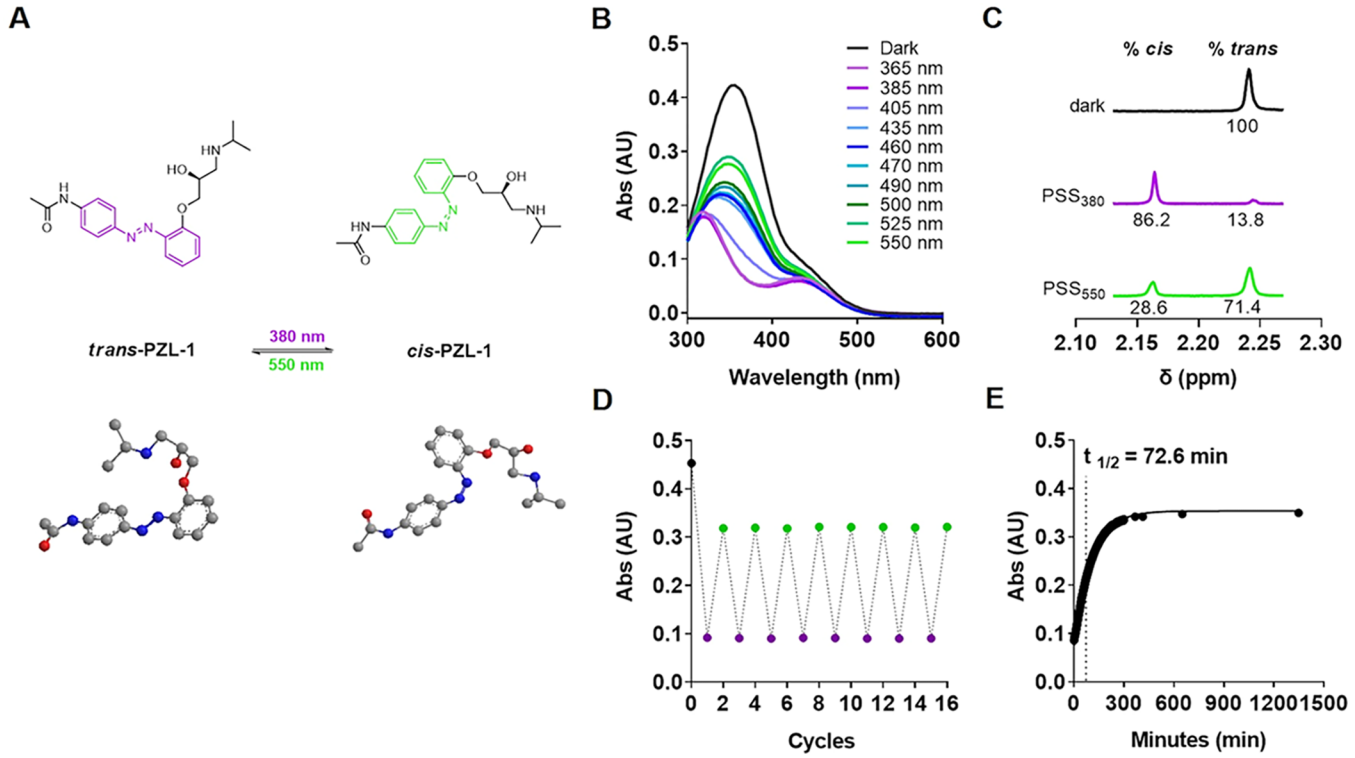

Figure 2. Photochemical evaluation of **PZL-1**. (A) Two-dimensional (2D) and three-dimensional (3D) chemical structures of the photoisomers of **PZL-1**. (B) UV−Vis absorption spectra of **PZL-1** under different light conditions. (C) Photostationary state (PSS) quantification by ^{1}H NMR. Samples were continuously illuminated using 380 and 550 nm light sources. Chemical shift variations on the methyl of the acetamide group were followed. (D) Multiple *cis*/*trans* isomerization cycles (380/550 nm) show the stability of the compound over 45 min of light application. (E) Half-life estimation of *cis*-**PZL-1** at 25 °C; the absorbance was measured at 364 nm.

lower efficiency, especially for **PZL-1** and **-2**, with conversions ranging from 71 to 77%. This can be explained through the shape of the UV−vis spectra of *trans* isomers. This family of compounds presents a strong $\pi-\pi^*$ band near 360 nm under dark conditions and a shoulder $n-\pi^*$ band at around 440 nm (Figure 2). The $n-\pi^*$ transition is forbidden by the symmetry in *trans* azobenzenes, which frequently leads to a spectrum with a very weak $n-\pi^*$ absorption band. Therefore, the presence of this slightly prominent $n-\pi^*$ band in the UV−vis spectrum of the *trans* isomer suggests that this transition is not completely forbidden for these compounds. This results in a non-negligible absorption of the *trans* isomers at these higher wavelengths and can be considered a particular feature in the UV−vis spectra of the described azobenzenes. In any case, this absorption hinders a more efficient light-triggered transition from *cis* toward the more thermodynamically stable *trans* isomer.

Moreover, thermal relaxation in aqueous media is relatively slow, considering that all measured half-lives at 25 °C are longer than 1 h (Table 1) and G protein activation happens on the second time scale.[31] Finally, photoisomerization of all compounds was found to be reversible and molecules were photostable over the application of multiple light cycles (Figures 2, S1, and S2).

Photopharmacological Characterization of Compounds. β_2-AR are primarily coupled to the G_s protein, which upon activation causes an increase of the intracellular concentration of cAMP through the regulation of adenylate cyclase.[32] Consequently, the biological activity of all compounds was evaluated through their ability to block the increase of intracellular cAMP induced by the addition of an agonist. An assay suitable to be employed under different illumination conditions was developed using a genetically encoded Epac CFP-YPF fluorescence resonance energy transfer (FRET) sensor that allowed to dynamically monitor intracellular concentrations of cAMP.[33] Briefly, a HEK293 cell line, which endogenously expresses β_2-AR, was transfected with the cAMP sensor and a single clone was selected to establish a stable cell line. These cells, which homogeneously express the target receptor and the cAMP sensor, were used to evaluate ligand light-dependent activities (Figure 3A).

We first evaluated the activity of the developed molecules under different light conditions. Dose−response curves were measured for **PZLs 1−3** supplemented with 3 nM cimaterol in dark conditions and under continuous illumination with violet light (Figures 3B,D and S6). Cimaterol was selected as a β_2-AR agonist for the assays considering that it is a potent ligand and has proved to be stable in aqueous solutions, even after 2 h of continuous illumination with near-ultraviolet light (Figure S7).[34] Remarkably, our results show that both **PZL-1** and **PZL-2** are potent β_2-AR antagonists with nanomolar activity (Table 2). On the other hand, their structural isomer **PZL-3** showed negligible antagonism (Figure S6). Strikingly, the light-dependent properties of the two active azobenzenes presented an opposite behavior (Figure 3A). Whereas the most thermodynamically stable configuration of **PZL-1** was found to be more potent (*trans*-on compound; Table 2), the *cis*-**PZL-2** demonstrated a significantly higher inhibition compared to its *trans* form (*cis*-on compound; Table 2). Indeed, **PZL-2** was found to be approximately 3.6 times more active upon illumination than in the dark. The light-induced shift in activity was noticeably higher for **PZL-1**, with a 17-fold shift of

https://dx.doi.org/10.1021/acs.jmedchem.0c00831
J. Med. Chem. 2020, 63, 8458−8470

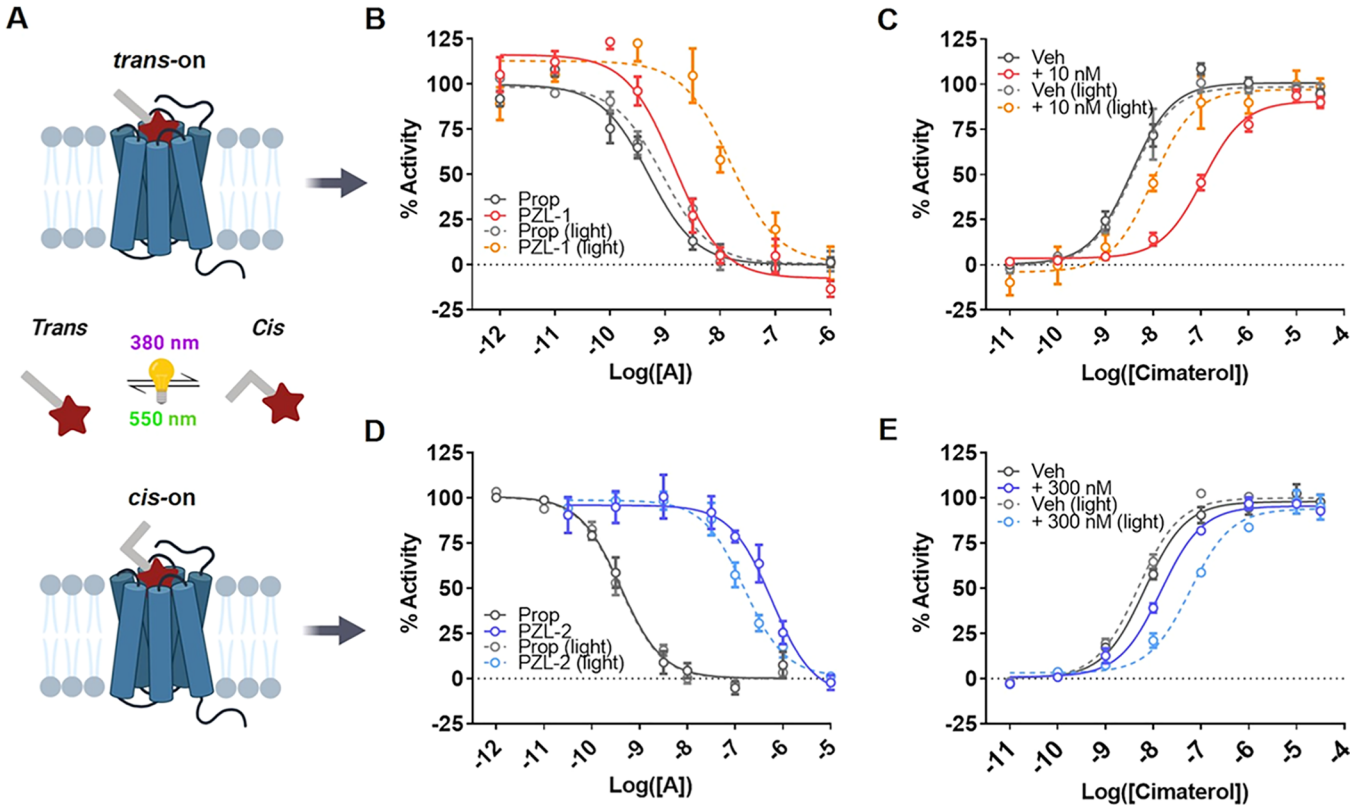

Figure 3. Light-dependent β_2-AR inhibition of **PZL-1** and **PZL-2**. (A) Representation of the two distinct photopharmacological behaviors observed for **PZL-1** (*trans*-on) and **PZL-2** (*cis*-on). Dose−response curves of **PZL-1** (B) and **PZL-2** (D) with a constant concentration of the agonist cimaterol (3 nM) in the dark and under constant violet light (380 nm). Dose−response curves of cimaterol in the presence of **PZL-1** (C) and **PZL-2** (E) in the dark and under constant violet light (380 nm). Data are shown as the mean ± SEM of four independent experiments in duplicate.

Table 2. Pharmacological Data of Photoswitchable β_2-AR Antagonists and Propranolol

	dark		light			
compound	IC_{50} (nM)	SEM	IC_{50} (nM)	SEM	shift[a]	SEM
PZL-1	1.72*	0.44	28.94	10.21	17.41	4.41
PZL-2	593.88****	35.73	160.64	23.20	0.28	0.05
PZL-3	>2000		>2000			
propranolol	0.55	0.13	0.48	0.11	0.97	0.21

[a]Relation between the measured IC_{50} in light and dark conditions, respectively. Statistical differences from light IC_{50} values are denoted for adjusted *p*-values as follows: $*p < 0.05$ and $****p < 0.0001$.

the inhibitory potency measured for the compound in dark conditions.

Finally, we aimed to corroborate that the measured antagonism for the two active azobenzenes was directly linked to β_2-AR. To do so, we performed analogous experiments on cells treated with forskolin, which induces an increase in cAMP concentration by activating adenylate cyclase instead of β_2-AR. In these experiments, no significant decrease of cAMP levels was observed for **PZL-1** or **PZL-2** (Figure S8), which demonstrates that the described antagonism is specific to the activation of β_2-AR by cimaterol.

To better characterize the light-dependent pharmacology of **PZL-1** and **PZL-2**, dose−response curves of the agonist were measured in the presence of different concentrations of the antagonist, both in dark and light conditions (Figures 3C,E, S9 and S10). The results confirm a competitive antagonism for both compounds and a light-triggered modulation of their potency. In particular, the addition of 10 nM **PZL-1** displaces 37-fold the dose−response curve of cimaterol to the right when cells are kept in the dark, whereas the EC_{50} variation is not significantly different to the control without **PZL-1** when the cells are illuminated (Table S1), thus validating the *trans*-on activity of this compound. On the other hand, the addition of 1 μM **PZL-2** shifts 20-fold the dose−response curve of cimaterol when cells are illuminated with violet light, whereas the curve displacement is significantly lower when cells are kept in the dark (Table S2). This further confirms the *cis*-on activity of **PZL-2**. For both compounds, a progressive increase in the concentration of the assayed compound produces equipotent displacements of the agonist curve and an increase of the agonist EC_{50} (Figures S9 and S10). Additionally, these experiments show no saturation of the inhibitory effect and no significant decrease of the maximal efficacy or basal activity, which is again consistent with a competitive antagonist pharmacological activity.

The development of compounds with opposing light-dependent pharmacology is of great interest since it provides a toolbox of compounds that enable the control of β_2-AR upon

https://dx.doi.org/10.1021/acs.jmedchem.0c00831
J. Med. Chem. 2020, 63, 8458−8470

illumination in different manners. Thus, **PZL-1**, blocking β_2-AR activity in the dark and allowing the receptor to be activated upon illumination, might be useful for certain research applications that require spatiotemporal activation of specific receptors while the rest remain inactive. In contrast, *cis*-on molecules like **PZL-2**, with increased inhibitory potency upon illumination, would allow a strict inactivation of a subset of receptors during a specific time while the rest remain under physiological conditions, which opens the door to the development of precise medical applications without side effects in other tissues and organs.

Dynamic and Reversible Photocontrol of β_2-AR. Probably, the most interesting and biologically unexplored capacity of photoisomerizable drugs acting on GPCRs is their ability to modulate the receptor activity over time using light as an externally operated regulatory control element of biological activity. For this to happen, it is necessary that the differential pharmacological effect of *cis* and *trans* states can be reverted and dynamically governed by means of light. In the present work, we addressed whether **PZL-1** and **PZL-2** were able to control the β_2-AR activation state with temporal precision.

First, we evaluated the time evolution of the receptor activity after treatment with the two active azobenzenes in dark and light conditions. To address this question, cells were incubated for 45 min with cimaterol and **PZL-1** or **PZL-2** in the dark and under violet illumination. After the incubation period, the activity of β_2-AR was continuously measured in the dark for 30 min (Figure S11). As expected, the experiments where **PZL-1** and **PZL-2** were kept in dark conditions showed a steady evolution of receptor activity over time. This indicates that both *trans* isomers have reached equilibrium after 45 min incubation. However, results after light application highlighted a remarkably different behavior for the two azobenzenes. At time zero, **PZL-1** shows a significantly higher inhibition of the receptor in dark conditions, consistent with the reduced activity measured for the *cis* isomer (Figures 3B and S11A). Continuous tracking of receptor activity for 30 min demonstrated that *cis*-**PZL-1** was spontaneously isomerizing to its thermodynamically stable *trans* isomer, as the antagonism was gradually restored over time. At the end of measurements, both illuminated and dark experiments showed similar levels of receptor activity. This suggests that **PZL-1** completely back-isomerized in the course of 30 min in the cell assay system, which is much faster than the measured relaxation time for the compound in a 0.5% DMSO buffer solution (Figure 2E). The increased thermal relaxation rate of *cis*-**PZL-1** in these experiments evidences a distinct photochemical behavior of the compound when it is enclosed in a more physiological environment. On the other hand, **PZL-2** was more efficient antagonizing the activity of cimaterol under violet illumination, which is aligned with its described *cis*-on behavior (Figures 3C and S11B). Interestingly, the antagonism observed for *cis*-**PZL-2** at time zero was maintained for the 30 min measured after illumination. This suggests that the interaction with the receptor stabilizes **PZL-2** in its *cis* isomer and leads to a reduced thermal relaxation rate to *trans*-**PZL-2**.

From the previous experiments, a question arises concerning the light-triggered reversibility of **PZL-1** and **PZL-2**, considering whether light is able to destabilize the ligand–receptor interaction once the active isomer is bound to β_2-AR. To address the temporal control of β_2-AR with light, in a subsequent series of experiments, we aimed to assess the capacity of **PZL-1** and **PZL-2** to dynamically modulate the receptor activation state using cycles of violet and green light (Figure 4). Interestingly, we found that receptor function

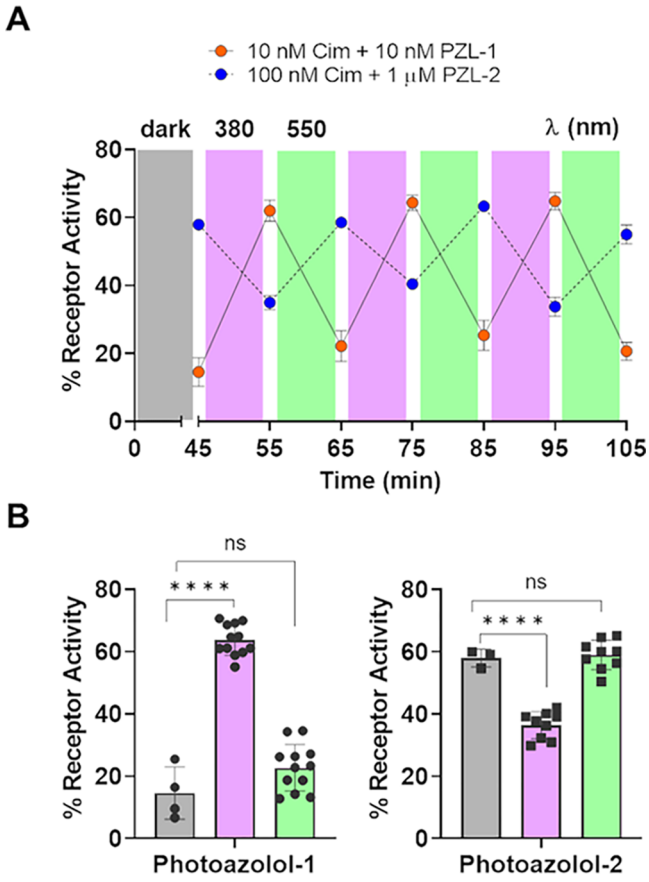

Figure 4. Real-time optical control of β_2-AR. (A) Time course quantification of intracellular cAMP challenged with the β_2-AR agonist cimaterol in the presence of **PZL-1** (orange dots) and **PZL-2** (blue dots). Purple and green boxes correspond to 10 min illumination breaks using 380 and 550 nm lights, respectively. (B) Receptor activity values measured for the different light conditions. Data are shown as the mean ± SEM of three to four independent experiments.

could be efficiently controlled in a reversible manner by the photoswitchable antagonists reported here through the application of intercalated light cycles at 380 and 550 nm. This β_2-AR reversible control *in vitro* was observed for at least three consecutive cycles. In particular, for the *trans*-on **PZL-1**, close to complete inhibition of the agonist was measured when it was coadded with cimaterol in the dark (Figure 4). This inhibitory effect was largely diminished when violet light was applied and could be restored upon the application of green light. The *cis*-on antagonist **PZL-2** showed a decrease of almost 30% on receptor activation when violet light was applied (Figure 4). This significant effect was completely reversed upon illumination with green light and this on/off cycle could be efficiently repeated several times with the same result. The described light-dependent effects were not observed when both azobenzenes were assayed in dark conditions, where the ligand activity remained stable throughout the course of the experiment (Figure S12).

These experiments demonstrate the potential and versatility of the developed photopharmacological tools to control the activity of β_2-AR, not only in space but also in time. Indeed,

https://dx.doi.org/10.1021/acs.jmedchem.0c00831
J. Med. Chem. 2020, 63, 8458–8470

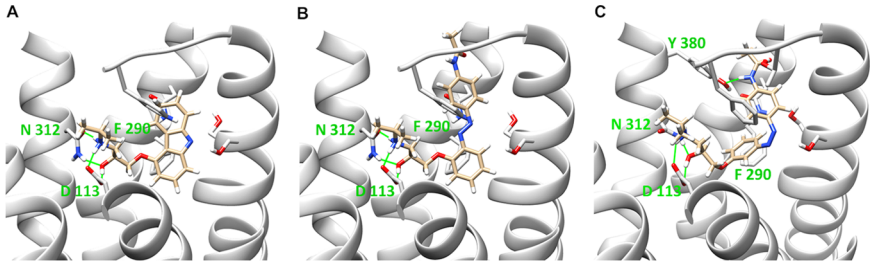

Figure 5. Binding mode of the active isomers of **PZL-1** and **PZL-2** in the crystal structure of human β_2-AR in complex with carazolol (PDB code 2RH1). (A) Rigid docking of carazolol in the empty receptor serves as a validation of the procedure. (B) Binding mode of *trans*-**PZL-1** within the orthosteric binding site of β_2-AR determined by rigid docking. (C) Binding mode of *cis*-**PZL-2** within the orthosteric binding site of β_2-AR determined by induced fit. Two amino acid positions (Asp113$^{3.32}$ and Asn312$^{7.39}$) are highlighted due to their importance in the binding of β_2-AR antagonists through a network of hydrogen bonds (represented by green lines).

one of the main differences between reversible photoswitches and other drug delivery methods is that the activity of reversible ligands can be pulsed with several on/off cycles. Therefore, the use of molecular photoswitches to reversibly control specific receptors may be used to resemble the dynamic control exerted in physiological regulatory processes. This particularity can also be extremely useful to uncover the role of a particular protein in a biological process[35] or to adapt a therapeutic treatment to the right time window and rhythm. Interestingly, the adaptation of a FRET biosensor to a photopharmacology assay has proven very useful to measure the functional activity of photoswitchable compounds in an endpoint mode, but it has also permitted to monitor the evolution of the ligand and light effects in the temporal dimension in a very simple manner. This has provided additional information about the interactions established between the ligand in both isomeric forms and the receptor. Moreover, this novel approach in photopharmacology has also enabled an assessment of the dynamic control of receptor activity through light cycles, which is essential for further research applications with **PZL-1** and **-2**.

Binding Modes of Active Photoisomers. To gain insight into the molecular interactions leading to the light-dependent effects of photoswitchable β_2-AR antagonists, we performed a computational study. We examined the binding mode of the different photoisomerizable molecules presented in this work using the crystal structure of the human β_2-AR in complex with carazolol (PDB code 2RH1).[36] This structure was chosen for the following reasons: first, it corresponds to the human β_2-AR, the same that was used in pharmacological assays; second, carazolol was used in the rational drug design of the azobenzene-based molecules investigated; and third, this crystal structure displays the highest resolution among all available β_2-AR structures.

Both, conventional rigid docking and induced fit protocols were used to introduce the small molecule in the pocket. Due to the planar geometry of the tricyclic carbazole moiety of carazolol, it was required the introduction of some flexibility in the receptor to allocate larger structures, such as the *cis* azobenzene. These procedures were previously validated by reintroducing carazolol in the empty pocket of the receptor with a very similar binding mode in comparison to the crystal structure (Figures 5A and S13D). The calculations performed with **PZL-3** did not retrieve any positive result neither by rigid docking nor by the induced fit protocol, which is in accordance with the lack of or very low activity measured for this compound in pharmacological assays (Figure S6). For **PZL-1** and **PZL-2**, several poses were obtained for both *cis* and *trans* isomers.

One of the most important molecular determinants for the affinity and activity of β_2-AR competitive antagonists is the formation of a hydrogen-bond network with the amino acids Asp113$^{3.32}$ and Asn312$^{7.39}$ (Figure 5). In our calculations, these interactions are conserved for all active photoisomers except for *trans*-**PZL-2**, which lacks one hydrogen bond with Asn312$^{7.39}$ (Figure S13). This may suggest that during the dynamics of the receptor the mentioned hydrogen bond is not as stable as when the molecule is in its *cis* form, in which this interaction is consistently found. This molecular feature may account for the light-triggered activity increase observed in pharmacological assays. Regarding **PZL-1**, both *trans*-**PZL-1** and *cis*-**PZL-1** configurations are forming the hydrogen-bond network (Figures 5B and S13E). However, in *trans*-**PZL-1**, these interactions are completely aligned with those found in the crystal structure for carazolol, whereas *cis*-**PZL-1** requires repositioning of several amino acids and the central part of the ligand. Interestingly, the *cis*-**PZL-1** interaction is found to be very similar to that of *cis*-**PZL-2** (Figure 5C), which is around 100-fold less potent than that of *trans*-**PZL-1**. These data suggest that both, *cis*-**PZL-1** and *cis*-**PZL-2**, may have very similar binding modes and thereafter present similar functional activities. Another remarkable difference found for the *cis*-binding of both molecules is the parallel offset aromatic interaction of the azobenzene ring with F290$^{6.52}$. This particular interaction is found to be T-shaped for carazolol, *trans*-**PZL-1**, and the majority of β_2-AR antagonists crystallized so far. Moreover, an additional hydrogen bond is formed between the two *cis* molecules and the hydroxyl group of Y308$^{7.35}$ residue in the upper part of the pocket, which may compensate for the loss of affinity in other regions (Figures 5C and S13E). Altogether, these data provide a molecular rationale aligned with the measured activities for the novel β_2-AR photoantagonists. Indeed, the nanomolar activity of the *trans*-**PZL-1** would suggest a very similar interaction pattern with the receptor compared to the cocrystalized carazolol. On the other hand, the *cis* isomers of both active azobenzenes interact with a noticeably different binding mode which decreases their activity but also provides an original new mode of interaction with the receptor. The novel binding mode comprises valuable knowledge that will facilitate the future design of new *cis*-on β_2-AR photoswitches. Further studies will be necessary to shed light on these novel interactions and to apply the highlighted concepts to the development of improved *cis*-on compounds.

https://dx.doi.org/10.1021/acs.jmedchem.0c00831
J. Med. Chem. 2020, 63, 8458−8470

CONCLUSIONS

The first proof of concept for a reversible β_2-AR photopharmacological approach is presented in this work. Following the azologization strategy, the hydrophobic moiety present in the majority of the β_2-AR antagonists was substituted for a *p*-acetamido azobenzene, which led to the development of two β_2-AR potent antagonists named **Photoazolol-1** and **-2**. Interestingly, **PZL-1** and **-2**, which are structural isomers, showed opposing light-regulated pharmacological properties. *Trans*-**PZL-1** was found to be the most active isomer, whereas for **PZL-2**, higher antagonism was observed on its *cis* form. Of note, we demonstrated that a dynamic control of the receptor activation with light is possible for both molecules. Additionally, a molecular rationale is provided to further explore the development of molecules with new photopharmacological and photochemical properties, such as red-shifted photoswitches that can be controlled with deep-penetrating wavelengths. Therefore, we have developed two chemical probes with complementary and reversible photochromic behavior, which opens the door to a broad range of future research applications. Further studies will be necessary to evaluate the selectivity of these and other photoswitchable β_2-AR antagonists for possible therapeutic uses and *in vivo* experiments. This confirmation would open the door to the study of specific roles of β_2-AR in pathophysiological processes, such as those involved in anxiety. Nonetheless, future research to shed light on the molecular mechanisms of β_2-AR signaling using fluorescence microscopy in combination with receptor photoswitching is assured. Overall, these potent tools enable the control of a prototypical class A GPCR enlarging the photopharmacological toolbox of compounds targeting the GPCR large family of proteins, which includes a substantial number of therapeutic targets.

EXPERIMENTAL SECTION

General Synthesis Methods. All starting materials were obtained from commercial sources and used without further purification unless otherwise stated. Anhydrous solvents were obtained from a solvent purification system (PureSolv-EN) and kept under a nitrogen atmosphere. Butanone was dried over activated molecular sieves prior to use. Reactions were monitored by thin-layer chromatography (TLC) on silica gel (60F, 0.2 mm, ALUGRAM Sil G/UV254, Macherey-Nagel) and visualized with 254 nm UV light. Flash column chromatography was carried using silica gel 60 (Panreac, 40−63 μm mesh) or by means of a Biotage Isolera One automated system with Biotage SNAP columns. Reactions under microwave irradiation were carried out in a CEM Discover Focused Microwave reactor. Reactions were performed in 10 mL sealed glass vessels. Analytical high-performance liquid chromatography (HPLC) was performed on a Thermo Ultimate 3000SD (Thermo Scientific Dionex) coupled to a PDA detector and an LTQ XL ESI-ion trap mass spectrometer (Thermo Scientific) or on a Waters 2795 Alliance coupled to a DAD detector (Agilent 1100) and an ESI Quattro Micro MS detector (Waters); HPLC columns used were ZORBAX Eclipse Plus C18 (4.6 × 150 mm; 3.5 μm) and ZORBAX Extend-C18 (2.1 × 50 mm, 3.5 μm). HPLC purity was determined using the following binary solvent system: 5% ACN in 0.05% formic acid for 0.5 min, from 5 to 100% ACN in 5 min, 100% ACN for 1.5 min, from 100 to 5% ACN in 2 min, and 5% ACN for 2 min. The flow rate was 0.5 mL/min, the column temperature was fixed to 35 °C, and wavelengths from 210 to 600 nm were registered. The purity of all compounds was determined to be >95%. NMR spectroscopy was performed using a Varian-Mercury 400 MHz spectrometer. Chemical shifts are reported in δ (ppm) relative to an internal standard (nondeuterated solvent signal). The following abbreviations have been used to designate multiplicities: s, singlet; d, doublet; t, triplet; m, multiplet; br, broad signal; dd, doublet of doublet; dt, doublet of triplet; ddd, doublet of doublet of doublet. Coupling constants (J) are reported in Hertz (Hz). HRMS and elemental composition were performed on a FIA with ultrahigh-performance liquid chromatography (UPLC) Aquity (Waters) coupled to LCT Premier Orthogonal Accelerated TOF (Waters). Data from mass spectra was analyzed by electrospray ionization in positive and negative modes using MassLynx 4.1 software (Waters), which provides a calculated mass with an additional electron. Spectra were scanned between 50 and 1500 Da with values every 0.2 s and peaks are reported as m/z. IR spectra were recorded neatly using a Thermo Nicolet Avatar 360 FT-IR spectrometer. Melting points were measured with a B-545 melting point instrument (Büchi). Optical rotation values were measured using a PerkinElmer 341 polarimeter with the indicated solvents. $[\alpha]_D$ values are reported in degrees and calculated as $c \times 100/(d \times m)$, where c is the concentration of the sample in g/100 mL, d is the optical way in dm, and m is the measured value (mean of five measurements). Chiral analytical HPLC was performed on a Thermo Ultimate 3000SD (Thermo Scientific Dionex) coupled to a Dionex VWD-3400-RS detector (Thermo Scientific; λ = 362 nm) or a Waters 1525 pump coupled to a Waters 2489 detector. As a chiral HPLC column, a Phenomenex Lux Amylose-2 (4.6 × 250 mm, 5 μM) was used. Enantiomeric excesses were determined using the following binary systems: (S1) 0.25% IPA + 0.3% DEA + 0.1% formic acid in ACN, isocratic; 0.5 mL/min; (S2) 0.5% IPA + 0.1% DEA + 0.1% formic acid in ACN, isocratic; 0.6 mL/min; and (S3) 1.5% IPA + 0.1% DEA in ACN, isocratic; 0.5 mL/min.

*1-Methoxy-3-nitrosobenzene (**2**).* A solution of oxone (11.0 g, 17.9 mmol) in water (20.3 mL) was added slowly to a solution of 3-methoxyaniline (**1**) (1.0 mL, 8.1 mmol) in DCM (20.3 mL). The reaction mixture was stirred vigorously at room temperature for approximately 2 h. The two phases were thereafter separated, and the aqueous layer was further extracted with DCM (15 mL × 3). The combined organic layers were washed with HCl (1 M), saturated Na_2CO_3, and brine. The organic extracts were dried over anhydrous $MgSO_4$, filtered, and evaporated under reduced pressure. The crude mixture was purified by flash column chromatography (hexane), and 1-methoxy-3-nitrosobenzene (**2**) (510 mg, 49%) was isolated as a green-red oil.

^{1}H NMR (400 MHz, chloroform-*d*) δ = 8.03 (ddd, J = 8, 2, 1.2 Hz, 1H), 7.59 (t, J = 8 Hz, 1H), 7.26 (ddd, J = 8, 2, 1.2 Hz, 1H), 6.89 (t, J = 2 Hz, 1H), 3.85 (s, 3H). The described NMR is in good agreement with the data reported in the literature.[37]

*N-(4-((3-Methoxyphenyl)diazenyl)phenyl)acetamide (**3**).* A suspension of 1-methoxy-3-nitrosobenzene (**2**) (510 mg, 3.7 mmol) and *N*-(4-aminophenyl)acetamide (559 mg, 3.7 mmol) in AcOH (7.4 mL) was left to stir overnight at room temperature. The crude was further purified by column chromatography (EtOAc/hexane 1:3), and compound **3** was isolated as an orange solid (410 mg, 41%), mp 145.6−145.8 °C.

^{1}H NMR (400 MHz, chloroform-*d*) δ = 7.92 (d, J = 8.8 Hz, 2H), 7.68 (d, J = 8.8 Hz, 2H), 7.53 (ddd, J = 8, 1.6, 0.8 Hz, 1H), 7.44−7.43 (m, 1H), 7.42 (t, J = 8 Hz, 1H), 7.32 (br, 1H), 7.03 (ddd, J = 8, 2.6, 0.8 Hz, 1H), 3.90 (s, 3H), 2.23 (s, 3H). ^{13}C NMR (101 MHz, chloroform-*d*) δ = 168.1, 160.5, 154.1, 149.1, 140.6, 129.9, 124.2, 119.8, 117.8, 117.2, 105.7, 55.6, 25.0. IR (neat): υ = 3298, 3252, 3190, 3125, 3064, 3004, 2937, 2833, 1665, 1590, 1544, 1501, 1406, 1319, 1264, 1148, 1123, 1041, 1031, 846, 782, 681. HRMS (ESI+): m/z calcd for $C_{15}H_{16}N_3O_2^+$ $[M + H]^+$ = 270.1243; found 270.1263.

*N-(4-Nitrosophenyl)acetamide (**9**).* Oxone (35.0 g, 56.9 mmol) was taken up in water (288 mL) and stirred vigorously at room temperature. Potassium carbonate (11.8 g, 85 mmol) was thereafter added slowly, and the resulting mixture was directly poured to a solution of *N*-(4-aminophenyl)acetamide (**4**) (4.27 g, 28.4 mmol) in water (423 mL). The reaction was left to stir for 10 min at room temperature, and a green precipitate was formed. The suspension was then filtered and dried. *N*-(4-Nitrosophenyl)acetamide (**9**) was isolated as a green solid (4.27 g, 91%) and used without further purification in the following reaction.

https://dx.doi.org/10.1021/acs.jmedchem.0c00831
J. Med. Chem. 2020, 63, 8458−8470

^{1}H NMR (400 MHz, DMSO-d_6) δ = 10.61 (br, 1H), 7.90−7.84 (m, 4H), 2.14 (s, 3H). The NMR spectrum is in good agreement to that reported in the literature.[38]

*N-(4-((2-Hydroxyphenyl)diazenyl)phenyl)acetamide (**10**).* A suspension of 2-aminophenol (1.064 g, 9.8 mmol) and *N*-(4-nitrosophenyl)acetamide (**9**) (1.6 g, 9.8 mmol) in AcOH (19.5 mL) was left to stir at room temperature for 48 h. The solvent was thereafter removed under reduced pressure to yield a black slurry. The residue was purified by column chromatography (EtOAc/hexane 1:3), and the product was isolated as a red solid (410 mg, 16%), mp 151.6−152.3 °C.

^{1}H NMR (400 MHz, chloroform-*d*) δ = 12.85 (s, 1H), 7.91 (dd, *J* = 8.1, 1.7 Hz, 1H), 7.86 (d, *J* = 8.8 Hz, 2H), 7.69 (d, *J* = 8.8 Hz, 2H), 7.33 (ddd, *J* = 8, 7.5, 1.7 Hz, 1H), 7.07 (ddd, *J* = 8, 7.5, 1.1 Hz, 1H), 7.02 (dd, *J* = 8.1, 1.1 Hz, 1H), 2.23 (s, 3H). IR (neat): υ = 3274, 3203, 3119, 2926, 1672, 1596, 1541, 1503, 1423, 1332, 1319, 1305, 1266, 843, 760, 751. HRMS (ESI+): *m*/*z* calcd for $C_{14}H_{14}N_3O_2^+$ $[M + H]^+$ = 256.1086 found 256.1079.

*N-(4-((3-Hydroxyphenyl)diazenyl)phenyl)acetamide (**5**).* A solution of *N*-(4-((3-methoxyphenyl)diazenyl)phenyl)acetamide **3** (450 mg, 1.7 mmol) in DCM (16.7 mL) was cooled down to 0 °C and kept under a nitrogen atmosphere. BBr_3 (1 M in DCM, 11.7 mL, 11.7 mmol) diluted in CH_2Cl_2 (6.3 mL) was added carefully, and the mixture was left to warm up and kept under constant stirring for 24 h. The reaction was terminated by the addition of water (50 mL). The mixture was left to stir for 1 h before the addition of 100 mL of EtOAc/MeOH (10:0.1). The two phases were separated, and the aqueous phase was further extracted with EtOAc (3 × 25 mL). The combined organic extracts were dried over Na_2SO_4, filtered, and concentrated under vacuum to yield an orange solid. Further purification was carried by column chromatography (EtOAc/hexane 1:3), and **5** was isolated as an orange solid (407 mg, 95%), mp 200.5−200.6 °C.

^{1}H NMR (400 MHz, methanol-d_4) δ = 7.86 (d, *J* = 8.8 Hz, 2H), 7.75 (d, *J* = 8.8 Hz, 2H), 7.39 (dt, *J* = 7.9, 1.5 Hz, 1H), 7.34 (t, *J* = 7.9 Hz, 1H), 7.29 (dd, *J* = 2.4, 1.7 Hz, 1H), 6.92 (ddd, *J* = 7.9, 2.4, 1.2 Hz, 1H), 2.17 (s, 3H). ^{13}C NMR (101 MHz, methanol-d_4) δ = 171.8, 159.4, 155.4, 150.0, 142.8, 130.9,124.6, 121.0, 119.1, 116.5, 108.8, 24.0. IR (neat): υ = 3404, 3066, 3018, 2860, 2725, 1660, 1602, 1585, 1525, 1504, 1469, 1435, 1407, 1389, 1307, 1258, 1236, 1157, 881, 840. HRMS (ESI+): *m*/*z* calcd for $C_{14}H_{14}N_3O_2^+$ $[M + H]^+$ = 256.1086; found 256.1096.

*N-(4-((4-Hydroxyphenyl)diazenyl)phenyl)acetamide (**6**).* *N*-(4-Aminophenyl)acetamide (**4**) (3.82 g, 25.4 mmol) was taken up in water (16.2 mL), and the solution was cooled down to −10 °C. HCl (15.5 mL, 509 mmol) was added carefully, and the mixture was left to stir for 5 min. A solution of sodium nitrite (3.95 g, 57.2 mmol) in water (24.2 mL) was then added dropwise through an addition funnel, keeping the temperature below 5 °C. The reaction was stirred for 10 min. In parallel, we prepared a solution of phenol (4.79 g, 50.9 mmol) in NaOH 10% (32.3 mL) and water (24.2 mL). This mixture was thereafter stirred vigorously and cooled down to −10 °C in an ice bath. The freshly prepared diazonium salt was kept cold to avoid degradation and was added very slowly on top of the phenolic solution. A red precipitate was formed immediately. The reaction mixture was allowed to stand in an ice bath for 30 min with occasional stirring, filtered, washed with water, and dried. Phenol **6** was isolated (4.1 g, 63%) as a brown solid, and no further purification was required, mp 181.9−184 °C.

^{1}H NMR (400 MHz, DMSO-d_6) δ = 10.24 (s, 1H), 7.82−7.71 (m, 6H), 6.92 (d, *J* = 8.4 Hz, 2H), 2.08 (s, 3H). ^{13}C NMR (101 MHz, DMSO-d_6) δ = 168.6, 160.5, 147.5, 145.3, 141.5, 124.5, 123.0, 119.1, 115.9, 24.1. NMR data are in good agreement with the literature.[39,40] IR (neat): υ = 3346, 3049, 2998, 2796, 2595, 1651, 1584, 1530, 1503, 1405, 1371, 1228, 1142, 835. HRMS (ESI +): *m*/*z* calcd for $C_{14}H_{14}N_3O_2^+$ $[M + H]^+$ = 256.1086; found 256.1061.

*(S)-N-(4-((2-(Oxiran-2-ylmethoxy)phenyl)diazenyl)phenyl)-acetamide (**11**). Method A.* *N*-(4-((2-Hydroxyphenyl)diazenyl)-phenyl)acetamide **10** (110 mg, 0.4 mmol) was taken up in anhydrous butanone (4.3 mL). K_2CO_3 (179 mg, 1.3 mmol) was added, and the suspension was left to stir for 10 min. (*R*)-epichlorohydrin (0.169 mL, 2.2 mmol) was finally added, and the reaction was heated to reflux overnight. An orange precipitate was formed. The suspension was thereafter filtered and washed with acetone (3 × 10 mL). Oxirane (*S*)-**11** was isolated as a red oil (98 mg, 73%).

^{1}H NMR (400 MHz, chloroform-*d*) δ = 7.91 (d, *J* = 8.8 Hz, 2H), 7.67 (d, *J* = 8.8 Hz, 2H), 7.66 (dd, *J* = 8.4, 1.6 Hz, 1H), 7.30 (br, 1H), 7.40 (ddd, *J* = 8.4, 7.2, 1.6 Hz, 1H), 7.12 (dd, *J* = 8.4, 1.2 Hz, 1H), 7.06 (ddd, *J* = 8.4, 7.2, 1.2 Hz, 1H), 4.46 (dd, *J* = 11.2, 3.1 Hz, 1H), 4.22 (dd, *J* = 11.2, 5.2 Hz, 1H), 3.44−3.48 (m, 1H), 2.93 (dd, *J* = 5.2, 4 Hz, 1H), 2.85 (dd, *J* = 5.2, 2.6 Hz, 1H), 2.22 (s, 3H). ^{13}C NMR (101 MHz, chloroform-*d*) δ = 168.4, 156.2,149.6, 143.0, 140.5, 132.2, 124.3, 122.0, 119.8, 117.3, 115.7, 70.9, 50.5, 45.0, 25.0. HRMS (ESI +): *m*/*z* calcd for $C_{17}H_{18}N_3O_3^+$ $[M + H]^+$ = 312.1348; found 312.1317.

Method B. *N*-(4-((2-Hydroxyphenyl)diazenyl)phenyl)acetamide **10** (65 mg, 0.2 mmol) was taken up in anhydrous DMF (5 mL). Potassium carbonate (34 mg, 0.2 mmol) was then added to the solution, and the mixture was left to stir under nitrogen for 10 min. (2*S*)-Glycidyl tosylate (46.5 mg, 0.2 mmol) was then added, and the reaction was left to stir overnight at room temperature. Oxirane **11** was not isolated and used directly on the subsequent step of the one-pot reaction.

*(S)-N-(4-((3-(Oxiran-2-ylmethoxy)phenyl)diazenyl)phenyl)-acetamide (**7**).* *N*-(4-((3-hydroxyphenyl)diazenyl)phenyl)acetamide **5** (250 mg, 0.98 mmol), was taken up in anhydrous butanone (9.8 mL). K_2CO_3 (406 mg, 2.94 mmol) was added, and the suspension was left to stir for 10 min. (*R*)-epichlorohydrin (384 μL, 4.90 mmol) was finally added, and the reaction was heated to reflux overnight. An additional equivalent of (*R*)-2-(chloromethyl)oxirane and K_2CO_3 was added, and the mixture was left to stir for 24 h. An orange precipitate was formed. The suspension was thereafter filtered and washed with acetone (3 × 10 mL). Oxirane **7** was isolated as a red oil (304 mg, 100%).

^{1}H NMR (400 MHz, chloroform-*d*) δ = 7.91 (d, *J* = 8.8 Hz, 2H), 7.67 (d, *J* = 8.8 Hz, 2H), 7.55 (ddd, *J* = 8.0, 1.7, 1 Hz, 1H), 7.43 (dd, *J* = 2.6, 1.7 Hz,1H), 7.41 (t, *J* = 8.0, 1H), 7.05 (ddd, *J* = 8.0, 2.6, 1 Hz, 1H), 4.33 (dd, *J* = 11.1, 3.1 Hz, 1H), 4.05 (dd, *J* = 11.1, 5.6 Hz, 1H), 3.38−3.42 (m,1H), 2.94 (dd, *J* = 5, 4.1 Hz, 1H), 2.80 (dd, *J* = 5, 2.6 Hz, 1H), 2.22 (s, 3H). ^{13}C NMR (101 MHz, chloroform-*d*) δ = 168.5, 159.3, 154.0, 149.0, 140.7, 130.0, 124.2, 119.8, 118.3, 117.9, 106.3, 69.0, 50.2, 44.9, 25.0. IR ($CHCl_3$): υ = 3311, 3193, 3126, 3065, 3006, 2928, 1672, 1596, 1538, 1503, 1406, 1371, 1317, 1302, 1259, 1150, 1123, 1037, 848, 753, 684. HRMS (ESI+): *m*/*z* calcd for $C_{17}H_{18}N_3O_3^+$ $[M + H]^+$ = 312.1348; found 312.1374. $[\alpha]_D^{25}$ = +5.6 (*c* = 1.0, $CHCl_3$). Racemic **7** (35 mg, 91%) was produced following the same protocol but using racemic epichlorohydrin (0.048 mL, 0.6 mmol).

*(S)-N-(4-((4-(Oxiran-2-ylmethoxy)phenyl)diazenyl)phenyl)-acetamide (**8**).* *N*-(4-((4-Hydroxyphenyl)diazenyl)phenyl)acetamide **6** (1.17 g, 4.6 mmol) was taken up in anhydrous butanone (11.5 mL). K_2CO_3 (1.9 g, 13.8 mmol) was added, and the suspension was left to stir for 10 min. (*R*)-epichlorohydrin (1.8 mL, 22.9 mmol) was finally added, and the reaction was heated to reflux overnight. An orange precipitate was observed. The suspension was thereafter filtered, washed with acetone (3 × 20 mL), and dried. Further purification was achieved by column chromatography (EtOAc/hexane 1:6), and oxirane **8** was isolated as a red solid (842 mg, 59%), mp 182.1−183.9 °C.

^{1}H NMR (400 MHz, DMSO-d_6) δ = 10.25 (s, 1H), 7.77−7.86 (m, 6H), 7.15 (d, *J* = 8.8 Hz, 2H), 4.45 (dd, *J* = 11.7, 2.6 Hz,1H), 3.94 (dd, *J* = 11.7, 6.6 Hz, 1H), 3.36−3.40 (m, 1H), 2.87 (t, *J* = 4.7 Hz, 1H), 2.74 (dd, *J* = 4.7, 2.6 Hz, 1H), 2.09 (s, 3H). ^{13}C NMR (101 MHz, DMSO-d_6) δ = 168.7, 160.5, 147.4, 146.4, 141.8, 124.2, 123.3, 119.1, 115.1, 69.4, 49.6, 43.8, 24.2. IR (neat): υ = 3302, 3258, 3192, 3126, 3074, 3004, 2912, 1667, 1591, 1539, 1497, 1367, 1299, 1255, 1242, 1152, 1031, 845, 826. HRMS (ESI+): *m*/*z* calcd for $C_{17}H_{18}N_3O_3^+$ $[M + H]^+$ = 312.1348; found 312.1329. $[\alpha]_D^{25}$ = +2.6 (*c* = 1.0, $CHCl_3$). (*R*)-**8** (703 mg, 90%) was produced following the same protocol but using (*S*)-epichlorohydrin (1.2 mL, 15.7 mmol).

https://dx.doi.org/10.1021/acs.jmedchem.0c00831
J. Med. Chem. 2020, 63, 8458−8470

*(S)-N-(4-((2-(2-Hydroxy-3-(isopropylamino)propoxy)phenyl)-diazenyl)phenyl)acetamide (**Photoazolol-1**). Method A.* (*S*)-*N*-(4-((2-(Oxiran-2-ylmethoxy)phenyl)diazenyl)phenyl)acetamide (**11**) (36 mg, 0.1 mmol) was dissolved in isopropylamine (0.5 mL, 5.8 mmol), and the reaction mixture was stirred at room temperature overnight. The reaction mixture was concentrated under reduced pressure, yielding 42 mg (100%) of orange oil identified as the product. Chiral HPLC showed that the compound was partially racemized when obtained by reaction with (*R*)-epichlorohydrin. Chiral HPLC (system 1): t_R = 15.0 min, ee 45%.

Method B. Oxirane **11** formed via the reaction of **10** with (2*S*)-glycidyl tosylate (Method B) was directly reacted with isopropylamine (0.175 mL, 2 mmol) in a one-pot reaction, and the mixture was heated up to 90 °C for 48 h. The reaction was then dried under vacuum, and water (20 mL) was added. The obtained solution was neutralized using 2 N NaOH and extracted using EtOAc (3 × 20 mL). The organic fractions were poured together, dried over anhydrous Na_2SO_4, filtered, and concentrated under reduced pressure. The product was further purified by automated column chromatography (water/ACN 95:5−0:100 + 0.05% HCOOH). The desired fractions were lyophilized to yield an orange solid, which was found to be the formiate salt of **PZL-1**. Neutralization was achieved through an aqueous workup using 1 N NaOH and EtOAc. **Photoazolol-1** was isolated as an orange oil (25 mg, 33%).

^{1}H NMR (400 MHz, chloroform-*d*) δ = 7.87 (d, *J* = 8.8 Hz, 2H), 7.67 (d, *J* = 8.8 Hz, 2H), 7.65 (dd, *J* = 8, 1.7 Hz, 1H), 7.59 (br, 1H), 7.41 (ddd, *J* = 8.4, 7.4, 1.7 Hz, 1H), 7.11 (dd, *J* = 8.4, 1.2 Hz, 1H), 7.06 (ddd, *J* = 8, 7.4, 1.2 Hz, 1H), 4.26−4.14 (m, 3H), 2.92 (dd, *J* = 12.1, 3.9 Hz, 1H), 2.88−2.81 (m, 2H), 2.21 (s, 3H), 1.07 (d, *J* = 6.3 Hz, 6H). ^{13}C NMR (101 MHz, chloroform-*d*) δ = 168.6, 156.1, 149.4, 143.2, 140.7, 132.4, 124.2, 122.2, 119.9, 117.8, 116.4, 73.8, 68.5, 49.3, 49.2, 24.9, 22.8, 22.7. IR ($CHCl_3$): υ = 3255, 2984, 1673, 1589, 1539, 1501, 1486, 1372, 1320, 1303, 1280, 1239, 1148, 1109, 1036, 846, 749, 665. HRMS (ESI+): *m*/*z* calcd for $C_{20}H_{27}N_4O_3^+$ $[M + H]^+$ = 371.2083; found 371.2064. Chiral HPLC (system 1): t_R = 14.9 min, ee 93%. $[\alpha]_D^{25}$ = − 61.4 (*c* = 1.0, MeOH).

*(S)-N-(4-((3-(2-Hydroxy-3-(isopropylamino)propoxy)phenyl)-diazenyl)phenyl)acetamide (**Photoazolol-2**).* (*S*)-*N*-(4-((3-(Oxiran-2-ylmethoxy)phenyl)diazenyl)phenyl)acetamide **7** (250 mg, 0.8 mmol) was dissolved in isopropylamine (3.4 mL, 40.1 mmol), and the reaction mixture was stirred at room temperature overnight. The solution was concentrated under reduced pressure and purified by reverse-phase automated column chromatography (water/ACN 95:5−0:100 + 0.05% HCOOH). The desired fractions were lyophilized to yield an orange solid, which was found to be the formiate salt of **PZL-2**. Neutralization was achieved through an aqueous workup using 1 N NaOH and EtOAc. **Photoazolol-2** was isolated as an orange oil (97.6 mg, 29%).

^{1}H NMR (400 MHz, chloroform-*d*) δ = 7.90 (d, *J* = 8.8, 2H), 7.67 (d, *J* = 8.8, 2H), 7.54 (ddd, *J* =8, 1.8, 1 Hz, 1H), 7.43 (dd, *J* = 1.8, 2.6 Hz, 1H), 7.40 (t, *J* = 8 Hz, 1H), 7.04 (ddd, *J* = 8, 2.6, 1.0 Hz, 1H), 4.07 (s, 3H), 2.90−2.95 (m, 1H), 2.86 (septet, *J* = 6.3 Hz, 1H), 2.79−2.73 (m, 1H), 2.22 (s, 3H), 1.11 (dd, *J* = 6.3 Hz, 6H). ^{13}C NMR (101 MHz, chloroform-*d*) δ = 168.5, 159.5, 154.0, 149.0, 140.7, 130.0, 124.2, 119.8, 118.1, 117.7, 106.3, 70.8, 68.5, 49.3, 49.2, 24.9, 23.2, 23.1. IR ($CHCl_3$): υ = 3305, 3195, 3125, 3065, 2967, 1673, 1594, 1539, 1503, 1405, 1370, 1317, 1303, 1257, 1215, 1150, 1127, 1037, 848, 749, 683. HRMS (ESI+): *m*/*z* calcd for $C_{20}H_{27}N_4O_3^+$ $[M + H]^+$ = 371.2083; found 371.2091. Chiral HPLC (system 2): t_R = 28.8 min, ee 88%. $[\alpha]_D^{25}$ = −3.6 (*c* = 1.0, MeOH). Racemic **PZL-2** (15 mg, 36%) was synthesized from racemic **7** (35 mg, 0.1 mmol) as described above.

*(S)-N-(4-((4-(2-Hydroxy-3-(isopropylamino)propoxy)phenyl)-diazenyl)phenyl)acetamide (**Photoazolol-3**).* (*S*)-*N*-(4-((4-(Oxiran-2-ylmethoxy)phenyl)diazenyl)phenyl)acetamide **8** (206 mg, 0.7 mmol) was dissolved in isopropylamine (2.8 mL, 33.1 mmol), and the reaction mixture was irradiated for 90 min in a microwave (100 °C, 200 psi, 200 W). CH_2Cl_2 (5 mL) was added to the orange solution, and a precipitate was formed. The suspension was filtered, washed with DCM (3 × 5 mL), and dried. **PZL-3** was obtained as an orange solid (137 mg, 56%), mp 159.5−163.2 °C.

^{1}H NMR (400 MHz, methanol-d_4) δ = 7.87 (d, *J* = 8.8 Hz, 2H), 7.84 (d, *J* = 8.8 Hz, 2H), 7.73 (d, *J* = 8.8 Hz, 2H), 7.09 (d, *J* = 8.8 Hz, 2H), 4.13−4.02 (m, 3H), 2.94−2.87 (m, 2H), 2.72 (dd, *J* = 12, 8.2 Hz, 1H), 2.16 (s, 3H), 1.13 (d, *J* = 3.6 Hz, 3H), 1.12 (d, *J* = 3.6 Hz, 3H). ^{13}C NMR (101 MHz, methanol-d_4) δ = 171.8, 162.7, 150.2, 148.4, 142.3, 125.5, 124.3, 121.0, 115.9, 72.2, 69.6, 50.6, 50.0, 24.0, 22.4, 22.3. IR (neat): υ = 3302, 3132, 2972, 2840, 1668, 1597, 1521, 1499, 1373, 1251, 1151, 1105, 1018, 845, 835. HRMS (ESI+): *m*/*z* calcd for $C_{20}H_{27}N_4O_3^+$ $[M + H]^+$ = 371.2083; found 371.2065. Chiral HPLC (system 3): t_R = 9.2 min, ee 99%. $[\alpha]_D^{25}$ = +6.6 (*c* = 1.0, MeOH). (*R*)-enantiomer of **PZL-3** (33 mg, 23%) was synthesized from (*R*)-**8** (123 mg, 0.4 mmol) as described above. Chiral HPLC (system 3): t_R = 9.6 min, ee 98%.

Photochemistry. *UV−Vis spectroscopy.* UV−vis spectra were recorded using a Tecan Spark 20M Multimode Microplate reader. All samples were prepared with 50 μM studied **PZL** in 0.5% DMSO cAMP EPAC sensor buffer (see below). Samples were measured between 600 and 300 nm with 2 nm fixed intervals in 96-well transparent plates (200 μL of compound solution/well). Illumination at different wavelengths was achieved using the CoolLED pE-4000 light source, set at 50% intensity. The liquid light guide accessory was pointed directly toward the well containing the studied sample for 3 min in continuous mode. CoolLED set at 50% intensity corresponded to 1.04 mW/mm^2 for 365 nm, 2.60 mW/mm^2 for 385 nm, 2.10 mW/mm^2 for 405 nm, 0.72 mW/mm^2 for 435 nm, 2.17 mW/mm^2 for 460 nm, 1.02 mW/mm^2 for 470 nm, 0.95 mW/mm^2 for 490 nm, 0.3 mW/mm^2 for 500 nm, 0.36 mW/mm^2 for 525 nm, and 1.57 mW/mm^2 for 550 nm light. Potencies were measured using a Thorlabs PM100D power energy meter connected with a standard photodiode power sensor (S120VC). Thermal relaxation studies were performed in the dark at 385 nm by prolonged absorbance measuring at 25 °C. The relaxation half-life of the compounds was calculated by plotting absorbance readings at λ = 364 nm vs time and by fitting the obtained curve to an exponential decay function. Multiple *trans*/*cis* isomerization cycles were registered by measuring absorbance at 364 nm in the dark and after 3 min of continuous illumination with 385 and 550 nm, respectively.

^{1}H NMR Photostationary State Determination. Data was acquired using a Bruker Avance-III 500 MHz spectrometer equipped with a *z*-axis pulsed-field gradient triple-resonance (^{1}H, ^{13}C, ^{15}N) TCI cryoprobe. 1D ^{1}H spectra were acquired at 285 K with 32 scans using the pulse sequence zgesgppe (water signal suppressed using excitation sculpting and perfect echo) extracted from the Bruker library. Every sample was locked, tuned, and shimmed prior to acquisition. External light was applied continuously for 3 min using the 96-well light-emitting diode (LED) array plate (LEDA Teleopto, Bio Research Center Co., Ltd.). Samples were prepared from a concentrated stock solution (10 mM in DMSO-d_6) by dilution in deuterated water (100 μM final). ^{1}H NMR spectrum of the compound in dark conditions was initially recorded. The sample was thereafter illuminated with 380 nm light in the NMR tube. ^{1}H NMR spectra were continuously collected over a period of 10−15 min to ensure there was no variation on PSS quantification attributed to thermal relaxation. The sample contained in the NMR tube was finally illuminated using 550 nm light. ^{1}H NMR spectra were again collected over a period of 10−15 min to assess the accuracy of PSS determination.

Cell Culture and transfection. The stable expressing cell line was established by limited dilution cloning. HEK293 cells were transfected with the Epac-S^{H188} biosensor (1 μg of H188 DNA) from the Kees Jalink group (Netherlands Cancer Institute) using X-tremeGENE 9 (Sigma-Aldrich, cat #6365787001, 3:1 X-tremeGENE/DNA ratio) as a transfecting agent. Transfection was carried in six-well Clear TC-treated multiple well plates (Corning, cat #3506) at a density of 500 000 cells/well. Cells were left to grow for 48 h before the selection process was started. The medium was then changed to D-glucose Dulbecco's modified Eagle medium (DMEM, GIBCO, cat #41965039) supplied with 10% heat-inactivated fetal bovine serum

https://dx.doi.org/10.1021/acs.jmedchem.0c00831
J. Med. Chem. 2020, 63, 8458−8470

(FBS; GIBCO, cat #11550356) containing 0.5 mg/mL Geneticin (G-418) to only select transfected cells. Two weeks after, cells were passaged and diluted in decreasing densities in a transparent 96-well plate (limited dilution cloning) using cell culture medium enriched with 0.5 μg/mL G-418. Three different single-cell colonies were isolated from this process. We assessed the functional activity of the three cell lines with the agonist cimaterol (see below), and the selected clone named HEK293-H188 M1 was found to be fluorescent, indicating the incorporation of the sensor. HEK293 cells stably expressing the Epac-S^{H188} cAMP biosensor were maintained at 37 °C, 5% CO_2 in DMEM supplied with 10% heat-inactivated FBS, and 1% penicillin−streptomycin (10 000 U/mL, GIBCO, cat #15140-122). Cells were split when reaching 75−90% confluence and detached by trypsin−ethylenediaminetetraacetic acid (EDTA; Sigma-Aldrich, cat #T3924) digestion.

Pharmacology. *General Data.* *In vitro* assays were carried out using HEK293 cells endogenously expressing β_2-AR and stably expressing the cAMP FRET biosensor. All assays were performed at room temperature. Adherent cells were grown in T-175 flasks or 150 mm dishes to 75−90% confluence. Cells were detached by rinsing once with PBS (GIBCO, cat #11550356), followed by incubation with trypsin−EDTA for 5 min until detachment of cells was observed. Cells were centrifugated at 1300 rpm for 3 min; in parallel, 10 μL of cell suspension were counted using a Neubauer Chamber. The supernatant was carefully removed, and cells were resuspended in DMEM complete medium to obtain a cell solution with 1.0 × 106 cells/mL. A density of 100 000 cells per well was seeded in a transparent 96-well microplate (Thermo Scientific Nunc Microwell, cat #10212811) and left at 37 °C with 5% CO_2 for approximately 24 h. The cAMP EPAC sensor buffer (14 mM NaCl, 50 nM KCl, 10 nM $MgCl_2$, 10 nM $CaCl_2$, 1 mM *N*-(2-hydroxyethyl)piperazine-*N*′-ethanesulfonic acid (HEPES), 1.82 mg/mL glucose, pH 7.2) was used as the assay medium in all FRET-based experiments. Fluorescence values were measured using a Tecan Spark M20 multimode microplate reader equipped with the Fluorescence Top Standard Module with defined wavelength settings (excitation filter 430/20 nm and emission filters 485/20 and 535/25 nm). The FRET ratio was calculated as the ratio of the donor emission ($td^{cp173}V$, 485 nm) to the acceptor emission (mTurq2Δ, 535 nm). The FRET ratio was normalized to the effect of the buffer (0%) and the maximum response obtained with cimaterol (100%). External light was applied using the 96-well LED array plate (LEDA Teleopto). Each set of experiments was performed three to five times with each concentration in duplicate or triplicate.

Stable Cell Line Characterization. A 96-well plate with the three isolated stable cell lines (HEK293-H188 M1, M2, and M3) was produced as described above. Cimaterol dose−response solutions were prepared in a preplate using the cAMP EPAC sensor buffer containing 100 μM IBMX. The culture medium was removed by inversion, and 90 μL of assay medium containing IBMX were added to the adherent cells. Different concentrations (10 μL) of the agonist were then added, and cells were left to incubate for 15 min at 25 °C. Fluorescence measurements were performed immediately after. FRET ratios were calculated and normalized to the effect of assay buffer (0%) and the maximum response obtained by cimaterol (100%). The experiments were performed in duplicate per cell line. To evaluate the sensor expression stability over time, two separate batches of cells stably expressing the biosensor were maintained under different selection conditions over 4 weeks. One of the batches was kept in DMEM complete medium, and the other in medium supplemented with 0.5 mg/mL G-418. The two cell batches were assayed (cimaterol dose−response assays) every week to assess the stability of sensor expression in a nonselective culture medium. No differences in activity were detected for more than a month. After these results, cells were maintained in DMEM complete medium with no additional antibiotics.

Cimaterol-Stimulated Assays. To perform the cimaterol-stimulated assays, we prepared two different plates, one for each light condition. For all assays, both plates were left to incubate with the studied compounds for 45 min at room temperature. To induce photoswitching, the "light plate" was exposed to continuous illumination (380 nm) during the incubation time using the LED array plate (LEDA Teleopto). Fluorescence values were thereafter measured for 30 min. Dose−response curves for each compound were obtained using a constant concentration of the agonist cimaterol (3.16 nM). Statistical analysis comparing the IC_{50} values of the compound in dark and light conditions was performed by unpaired Student's *t*-test. To see the effect of the antagonists on the agonist dose−response, dose−response curves for cimaterol were prepared in combination with different constant concentrations of the photoswitchable compound (up to 10 nM **PZL-1** and 1 μM **PZL-2**). Statistical analysis of the differences between the vehicle and the assayed concentrations of **PZLs**, pairwise comparisons based on the extra sum-of-squares *F* test for Log(EC_{50}) were performed. The obtained p-values were corrected using a multiple testing method known as the false discovery rate (FDR).[41] Differences between curves with an equal concentration of **PZL** under the different light conditions were analyzed via an extra sum-of-squares *F* test followed by an FDR test.

Forskolin-Stimulated Assays. To evaluate that the activity of the synthesized antagonists was directly linked to β_2-AR, we stimulated the cells using forskolin, a described activator of adenyl cyclase. For each experiment, we prepared two different plates, one for each light condition. Dose−response curves for each compound were obtained using a constant concentration of forskolin (10 μM). Dose−response curves of forskolin were also evaluated with a constant concentration of the photoswitchable compounds (up to 10 nM **PZL-1** and 1 μM **PZL-2**). Both plates were left to incubate with the assayed compounds for 45 min at room temperature. To induce photoswitching, the light plate was exposed to continuous illumination (380 nm) with the LED array plate (LEDA Teleopto) during the incubation time. Fluorescence values were thereafter recorded for 30 min.

Real-Time Assays. Assays to assess the dynamic control of receptor activity were carried out using a constant concentration of azobenzene and cimaterol (1 μM **PZL-1**/100 nM cimaterol and 10 nM **PZL-2**/10 nM cimaterol). Cellular response to buffer and buffer supplemented with cimaterol (100 and 10 nM) was also evaluated. Cells were left to incubate with the compounds for 45 min, and fluorescence was measured. Then, the plate was continuously illuminated with light at 380 nm for 10 min and fluorescence values were recorded. Immediately after, the plate was illuminated in continuous mode for 10 min with light at 550 nm and fluorescence was measured. Two additional light cycles were applied to ensure the reversibility in receptor activity triggered by light was reproducible over time. Statistical analysis comparing the three light conditions was performed by a one-way analysis of variance (ANOVA) followed by Tukey's multiple comparisons test.

Data Analysis. All experiments were analyzed using GraphPad Prism 8.1.1 (GraphPad Software, San Diego, CA). Stimulation dose−response data was fitted using the log(agonist) vs response (three parameters) function. Inhibition dose−response data was fitted using the log (antagonist) vs response (three parameters) function. For FDR tests, Stata 15.0 was used (StataCorp. 2017. Stata: Release 15. Statistical Software. College Station, TX: StataCorp LLC). Unless stated, data was analyzed using ANOVA, extra sum-of-squares *F* test, or unpaired Student's *t*-test (see the different sections).

Molecular Modeling. The crystal structure of the human β_2-AR in complex with carazolol was retrieved from the Protein Data Bank (PDB code 2RH1) and used to examine the binding mode of each molecule. Molecular calculations were performed in Maestro (Schrödinger Release 2020-1: Maestro, Schrödinger, LLC, New York, NY, 2020). For each photoisomerizable molecule, *cis* and *trans* configurations were generated and prepared for the calculation with Ligprep using the forcefield OPLS3e and retaining the specified chiralities. Then, both rigid (Glide) and induced fit docking protocols were used to evaluate the interaction of molecules centered in the binding site of carazolol. In the Induced fit protocol, an initial Glide docking was performed. The receptor and ligand Van der Waals scaling was set to 0.50, and the maximum number of poses to 20. A

https://dx.doi.org/10.1021/acs.jmedchem.0c00831
J. Med. Chem. 2020, 63, 8458−8470

refinement of residues within 5 Å of ligand poses was performed by Prime. Finally, Glide redocking was carried out into structures within 30 kcal/mol of the best structure and within the top 20 best structures overall. The evaluation of results was done by ranking all poses using the Glide score and by visual inspection.

■ ASSOCIATED CONTENT

Supporting Information

The Supporting Information is available free of charge at https://pubs.acs.org/doi/10.1021/acs.jmedchem.0c00831.

Compound characterization spectra, additional photochemical and pharmacological data, NMR data on the photostationary state quantification experiments, chemical stability of the agonist cimaterol upon illumination, and additional computational calculations (PDF)
Dockings (ZIP)
Molecular formula strings (CVS)

■ AUTHOR INFORMATION

Corresponding Authors

Xavier Rovira − *Molecular Photopharmacology Research Group, The Tissue Repair and Regeneration Laboratory (TR2Lab), Faculty of Sciences and Technology, University of Vic—Central University of Catalonia, 08500 Barcelona, Spain;* orcid.org/0000-0002-9764-9927; Email: xavier.rovira@iqac.csic.es

Amadeu Llebaria − *MCS, Laboratory of Medicinal Chemistry, Institute for Advanced Chemistry of Catalonia (IQAC-CSIC), 08034 Barcelona, Spain;* orcid.org/0000-0002-8200-4827; Email: amadeu.llebaria@iqac.csic.es

Authors

Anna Duran-Corbera − *MCS, Laboratory of Medicinal Chemistry, Institute for Advanced Chemistry of Catalonia (IQAC-CSIC), 08034 Barcelona, Spain*

Juanlo Catena − *MCS, Laboratory of Medicinal Chemistry and SiMChem, Service of Synthesis of High Added Value Molecules, Institute for Advanced Chemistry of Catalonia (IQAC-CSIC), 08034 Barcelona, Spain*

Marta Otero-Viñas − *Molecular Photopharmacology Research Group, The Tissue Repair and Regeneration Laboratory (TR2Lab), Faculty of Sciences and Technology, University of Vic—Central University of Catalonia, 08500 Barcelona, Spain*

Complete contact information is available at: https://pubs.acs.org/10.1021/acs.jmedchem.0c00831

Notes

The authors declare no competing financial interest.

■ ACKNOWLEDGMENTS

We thank Montserrat Masoliver (UVic-UCC, Vic, Spain), Joan Bertrán (UVic-UCC, Vic, Spain), Jordi Serra (UVic-UCC, Vic, Spain), Lourdes Muñoz (SiMChem, IQAC-CSIC, Barcelona), Maria José Bleda (IQAC-CSIC, Barcelona), Ignacio Pérez (IQAC-CSIC, Barcelona), Yolanda Pérez (IQAC-CSIC, Barcelona), and Carme Serra (SiMChem, IQAC-CSIC, Barcelona) for technical support. We thank Dr. Kees Jalink (The Netherlands Cancer Institute, Amsterdam, the Netherlands) for providing the plasmids encoding for the Epac-S^{H188} biosensor. We thank the Cisbio Bioassays for their support and technical discussion, as well as for providing plasmids for the preliminary optimization of the biological assays. The project that gave rise to these results received the support of a fellowship from "la Caixa" Foundation (ID 100010434) under the fellowship code LCF/BQ/DE18/11670012. This work was supported by FEDER/Ministerio de Ciencia, Innovación y Universidades-Agencia Estatal de Investigación (CTQ2017-89222-R), the Catalan Government (2017SGR1604), PO FEDER of Catalonia 2014−2020 (project PECT Osona Transformació Social, ref 001-P-000382), and the Spanish Ministry of Economy, Industry and Competitiveness (SAF2015-74132-JIN).

■ ABBREVIATIONS

CFP, cyan fluorescent protein; YFP, yellow fluorescent ptotein; HEK293 cells, human embryonic kindey 293 cells; FBS, fetal bovine serum; SEM, standard error of the mean; DAD, diode array detector; PDA, photodiode array detector; LED, light-emitting diode; IBMX, 1,3-isobutyl-1-methoxyxanthine; IPA, isopropylamine; DEA, diethylamine; HEPES, (4-(2-hydroxyethyl)-1-piperazineethanesulfonic acid)

■ REFERENCES

(1) Lerch, M. M.; Hansen, M. J.; van Dam, G. M.; Szymanski, W.; Feringa, B. L. Emerging Targets in Photopharmacology. *Angew. Chem., Int. Ed.* **2016**, *55*, 10978−10999.

(2) Ricart-Ortega, M.; Font, J.; Llebaria, A. GPCR Photopharmacology. *Mol. Cell. Endocrinol.* **2019**, *488*, 36−51.

(3) Zussy, C.; Gómez-Santacana, X.; Rovira, X.; De Bundel, D.; Ferrazzo, S.; Bosch, D.; Asede, D.; Malhaire, F.; Acher, F.; Giraldo, J.; Valjent, E.; Ehrlich, I.; Ferraguti, F.; Pin, J. P.; Llebaria, A.; Goudet, C. Dynamic Modulation of Inflammatory Pain-Related Affective and Sensory Symptoms by Optical Control of Amygdala Metabotropic Glutamate Receptor 4. *Mol. Psychiatry* **2018**, *23*, 509−520.

(4) Font, J.; López-Cano, M.; Notartomaso, S.; Scarselli, P.; Di Pietro, P.; Bresolí-Obach, R.; Battaglia, G.; Malhaire, F.; Rovira, X.; Catena, J.; Giraldo, J.; Pin, J.-P.; Fernández-Dueñas, V.; Goudet, C.; Nonell, S.; Nicoletti, F.; Llebaria, A.; Ciruela, F. Optical Control of Pain in Vivo with a Photoactive $MGlu_5$ Receptor Negative Allosteric Modulator. *Elife* **2017**, *6*, No. e23545.

(5) Hüll, K.; Morstein, J.; Trauner, D. In Vivo Photopharmacology. *Chem. Rev.* **2018**, *118*, 10710−10747.

(6) Ellis-Davies, G. C. R. Caged Compounds: Photorelease Technology for Control of Cellular Chemistry and Physiology. *Nat. Methods* **2007**, *4*, 619−628.

(7) Hoorens, M. W. H.; Szymanski, W. Reversible, Spatial and Temporal Control over Protein Activity Using Light. *Trends Biochem. Sci.* **2018**, *43*, 567−575.

(8) Morstein, J.; Awale, M.; Reymond, J. L.; Trauner, D. Mapping the Azolog Space Enables the Optical Control of New Biological Targets. *ACS Cent. Sci.* **2019**, *5*, 607−618.

(9) Gómez-Santacana, X.; de Munnik, S. M.; Vijayachandran, P.; Da Costa Pereira, D.; Bebelman, J. P. M.; de Esch, I. J. P.; Vischer, H. F.; Wijtmans, M.; Leurs, R. Photoswitching the Efficacy of a Small-Molecule Ligand for a Peptidergic GPCR: From Antagonism to Agonism. *Angew. Chem., Int. Ed.* **2018**, *57*, 11608−11612.

(10) Gómez-Santacana, X.; Pittolo, S.; Rovira, X.; Lopez, M.; Zussy, C.; Dalton, J. A. R.; Faucherre, A.; Jopling, C.; Pin, J. P.; Ciruela, F.; Goudet, C.; Giraldo, J.; Gorostiza, P.; Llebaria, A. Illuminating Phenylazopyridines to Photoswitch Metabotropic Glutamate Receptors: From the Flask to the Animals. *ACS Cent. Sci.* **2017**, *3*, 81−91.

(11) Donthamsetti, P. C.; Winter, N.; Schönberger, M.; Levitz, J.; Stanley, C.; Javitch, J. A.; Isacoff, E. Y.; Trauner, D. Optical Control of Dopamine Receptors Using a Photoswitchable Tethered Inverse Agonist. *J. Am. Chem. Soc.* **2017**, *139*, 18522−18535.

(12) Bahamonde, M. I.; Taura, J.; Paoletta, S.; Gakh, A. A.; Chakraborty, S.; Hernando, J.; Fernández-Dueñas, V.; Jacobson, K. A.; Gorostiza, P.; Ciruela, F. Photomodulation of G Protein-Coupled Adenosine Receptors by a Novel Light-Switchable Ligand. *Bioconjugate Chem.* **2014**, *25*, 1847−1854.

(13) Agnetta, L.; Kauk, M.; Canizal, M. C. A.; Messerer, R.; Holzgrabe, U.; Hoffmann, C.; Decker, M. A Photoswitchable Dualsteric Ligand Controlling Receptor Efficacy. *Angew. Chem., Int. Ed.* **2017**, *56*, 7282−7287.
(14) Lachmann, D.; Studte, C.; Männel, B.; Hübner, H.; Gmeiner, P.; König, B. Photochromic Dopamine Receptor Ligands Based on Dithienylethenes and Fulgides. *Chem. - Eur. J.* **2017**, *23*, 13423−13434.
(15) Riefolo, F.; Matera, C.; Garrido-Charles, A.; Gomila, A. M. J.; Sortino, R.; Agnetta, L.; Claro, E.; Masgrau, R.; Holzgrabe, U.; Batlle, M.; Decker, M.; Guasch, E.; Gorostiza, P. Optical Control of Cardiac Function with a Photoswitchable Muscarinic Agonist. *J. Am. Chem. Soc.* **2019**, *141*, 7628−7636.
(16) Schönberger, M.; Trauner, D. A Photochromic Agonist for μ-Opioid Receptors. *Angew. Chem., Int. Ed.* **2014**, *53*, 3264−3267.
(17) Westphal, M. V.; Schafroth, M. A.; Sarott, R. C.; Imhof, M. A.; Bold, C. P.; Leippe, P.; Dhopeshwarkar, A.; Grandner, J. M.; Katritch, V.; Mackie, K.; Trauner, D.; Carreira, E. M.; Frank, J. A. Synthesis of Photoswitchable9-Tetrahydrocannabinol Derivatives Enables Optical Control of Cannabinoid Receptor 1 Signaling. *J. Am. Chem. Soc.* **2017**, *139*, 18206−18212.
(18) Hauwert, N. J.; Mocking, T. A. M.; Da Costa Pereira, D.; Kooistra, A. J.; Wijnen, L. M.; Vreeker, G. C. M.; Verweij, E. W. E.; De Boer, A. H.; Smit, M. J.; De Graaf, C.; Vischer, H. F.; De Esch, I. J. P.; Wijtmans, M.; Leurs, R. Synthesis and Characterization of a Bidirectional Photoswitchable Antagonist Toolbox for Real-Time GPCR Photopharmacology. *J. Am. Chem. Soc.* **2018**, *140*, 4232−4243.
(19) Santos, R.; Ursu, O.; Gaulton, A.; Bento, A. P.; Donadi, R. S.; Bologa, C. G.; Karlsson, A.; Al-Lazikani, B.; Hersey, A.; Oprea, T. I.; Overington, J. P. A Comprehensive Map of Molecular Drug Targets. *Nat. Rev. Drug Discovery* **2016**, *16*, 19−34.
(20) Baker, J. G.; Hill, S. J.; Summers, R. J. Evolution of β-Blockers: From Anti-Anginal Drugs to Ligand-Directed Signalling. *Trends Pharmacol. Sci.* **2011**, *32*, 227−234.
(21) Yadav, K. S.; Rajpurohit, R.; Sharma, S. Glaucoma: Current Treatment and Impact of Advanced Drug Delivery Systems. *Life Sci.* **2019**, *221*, 362−376.
(22) Muralidharan, S.; Nerbonne, J. M. Photolabile "Caged" Adrenergic Receptor Agonists and Related Model Compounds. *J. Photochem. Photobiol., B* **1995**, *27*, 123−137.
(23) Mu, C.; Shi, M.; Liu, P.; Chen, L.; Marriott, G. Daylight-Mediated, Passive, and Sustained Release of the Glaucoma Drug Timolol from a Contact Lens. *ACS Cent. Sci.* **2018**, *4*, 1677−1687.
(24) Siuda, E. R.; McCall, J. G.; Al-Hasani, R.; Shin, G.; Park, S. Il.; Schmidt, M. J.; Anderson, S. L.; Planer, W. J.; Rogers, J. A.; Bruchas, M. R. Optodynamic Simulation of β-Adrenergic Receptor Signalling. *Nat. Commun.* **2015**, *6*, No. 8480.
(25) Chan, H. C. S.; Filipek, S.; Yuan, S. The Principles of Ligand Specificity on Beta-2-Adrenergic Receptor. *Sci. Rep.* **2016**, *6*, No. 34736.
(26) Broichhagen, J.; Frank, J. A.; Trauner, D. A Roadmap to Success in Photopharmacology. *Acc. Chem. Res.* **2015**, *48*, 1947−1960.
(27) Mehvar, R.; Brocks, D. R. Stereospecific Pharmacokinetics and Pharmacodynamics of Beta-Adrenergic Blockers in Humans. *J. Pharm. Pharm. Sci.* **2001**, *4*, 185−200.
(28) Dong, M.; Babalhavaeji, A.; Samanta, S.; Beharry, A. A.; Woolley, G. A. Red-Shifting Azobenzene Photoswitches for in Vivo Use. *Acc. Chem. Res.* **2015**, *48*, 2662−2670.
(29) McClure, D. E.; Arison, B. H.; Baldwin, J. J. Mode of Nucleophilic Addition to Epichlorohydrin and Related Species: Chiral Aryloxymethyloxiranes. *J. Am. Chem. Soc.* **1979**, *101*, 3666−3668.
(30) Klunder, J. M.; Ko, S. Y.; Sharpless, K. B. Asymmetric Epoxidation of Allyl Alcohol: Efficient Routes to Homochiral/3-Adrenergic Blocking Agents. *J. Org. Chem.* **1986**, *51*, 3710−3712.
(31) Masuho, I.; Ostrovskaya, O.; Kramer, G. M.; Jones, C. D.; Xie, K.; Martemyanov, K. A. Distinct Profiles of Functional Discrimination among G Proteins Determine the Actions of G Protein-Coupled Receptors. *Sci. Signal.* **2015**, *8*, No. ra123.
(32) Stiles, G. L.; Caron, M. G.; Lefkowitz, R. J. β-Adrenergic Receptors: Biochemical Mechanisms of Physiological Regulation. *Physiol. Rev.* **1984**, *64*, 661−743.
(33) Klarenbeek, J.; Goedhart, J.; Van Batenburg, A.; Groenewald, D.; Jalink, K. Fourth-Generation Epac-Based FRET Sensors for CAMP Feature Exceptional Brightness, Photostability and Dynamic Range: Characterization of Dedicated Sensors for FLIM, for Ratiometry and with High Affinity. *PLoS One* **2015**, *10*, No. e0122513.
(34) Baker, J. G.; Gardiner, S. M.; Woolard, J.; Fromont, C.; Jadhav, G. P.; Mistry, S. N.; Thompson, K. S. J.; Kellam, B.; Hill, S. J.; Fischer, P. M. Novel Selective B1-Adrenoceptor Antagonists for Concomitant Cardiovascular and Respiratory Disease. *FASEB J.* **2017**, *31*, 3150−3166.
(35) Sandoz, G.; Levitz, J.; Kramer, R. H.; Isacoff, E. Y. Optical Control of Endogenous Proteins with a Photoswitchable Conditional Subunit Reveals a Role for TREK1 in GABAB Signaling. *Neuron* **2012**, *74*, 1005−1014.
(36) Cherezov, V.; Rosenbaum, D. M.; Hanson, M. A.; Rasmussen, S. G. F.; Foon, S. T.; Kobilka, T. S.; Choi, H. J.; Kuhn, P.; Weis, W. I.; Kobilka, B. K.; Stevens, R. C. High-Resolution Crystal Structure of an Engineered Human B2-Adrenergic G Protein-Coupled Receptor. *Science* **2007**, *318*, 1258−1265.
(37) Molander, G. A.; Cavalcanti, L. N. Nitrosation of Aryl and Heteroaryltrifluoroborates with Nitrosonium Tetrafluoroborate. *J. Org. Chem.* **2012**, *77*, 4402−4413.
(38) Bujak, K.; Nocoń, K.; Jankowski, A.; Wolińska-Grabczyk, A.; Schab-Balcerzak, E.; Janeczek, H.; Konieczkowska, J. Azopolymers with Imide Structures as Light-Switchable Membranes in Controlled Gas Separation. *Eur. Polym. J.* **2019**, *118*, 186−194.
(39) Lerch, M. M.; Hansen, M. J.; Velema, W. A.; Szymanski, W.; Feringa, B. L. Orthogonal Photoswitching in a Multifunctional Molecular System. *Nat. Commun.* **2016**, *7*, No. 12054.
(40) Mutter, N. L.; Volarić, J.; Szymanski, W.; Feringa, B. L.; Maglia, G. Reversible Photocontrolled Nanopore Assembly. *J. Am. Chem. Soc.* **2019**, *141*, 14356−14363.
(41) Benjamini, Y.; Hochberg, Y. Controlling the False Discovery Rate: A Practical and Powerful Approach to Multiple Testing. *J. R. Stat. Soc. Series B Stat. Methodol.* **1995**, *57*, 289−300.

https://dx.doi.org/10.1021/acs.jmedchem.0c00831
J. Med. Chem. 2020, 63, 8458−8470